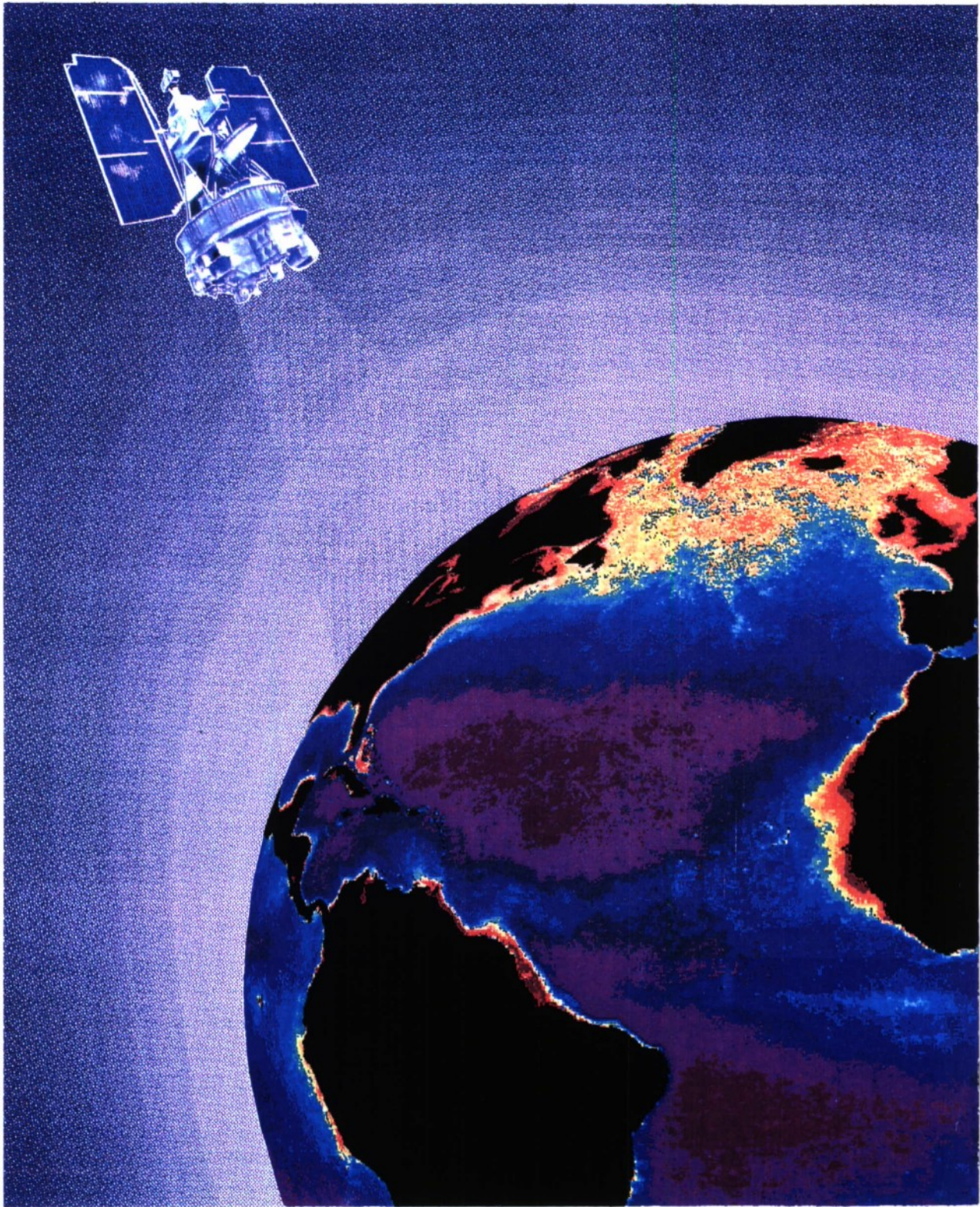


Naval Oceanographic and Atmospheric Research Laboratory
Stennis Space Center, Mississippi 39529-5004

~~NAVY~~
~~RESEARCH REPORTS DIVISION~~
~~NAVAL POSTGRADUATE SCHOOL~~
~~MONTEREY, CA 93943-5002~~



Applications of Ocean Color to Naval Warfare

G. Daniel Hickman
Editor

0314858

Robert A. Arnone

James L. Mueller

Optical Climatologies

Abstract: Satellite-derived ocean color data yield global information on optical properties of the ocean. This information is important in predicting the performance of various Navy electro-optical systems. Although optical climatologies are valuable for planning various Navy applications, real-time, satellite-derived, ocean optical parameters are paramount to the effective operation of many weapon systems.

Significant advances in optical oceanography have recently been made by using satellite-derived ocean color data. The Coastal Zone Color Scanner (CZCS) data base provided the first global overview of the spatial and temporal distributions of near-surface bio-optical properties (Austin and Petzold, 1981; Smith and Baker, 1978, 1982; Gordon et al., 1980, 1983) and scales of variability. In deep-ocean Case I waters, where the concentration of phytoplankton is high compared to that of other particles (Morel and Prieur, 1977), optical properties vary seasonally and co-vary with surface phytoplankton concentrations.

In open-ocean frontal areas and in coastal waters, satellite ocean color data reveal a more spatially complex and temporally variable structure than had been envisioned. The academic research community is aggressively pursuing research to use the spatial and temporal information in global ocean color climatologies. This information will allow global primary productivity and related processes that control the carbon-dioxide and other biogeochemical cycles in the ocean-atmosphere-terrestrial system to be better quantified and understood. Ocean color data from the forthcoming SeaWiFS figure prominently in planning for Joint Global Ocean Flux Study (JGOFS) research over the coming decade.

For many Navy applications, ocean color climatologies based on the CZCS (and the SeaWiFS) data provide estimates of regional ocean optical properties and of variability on mesoscale, seasonal, and regional scales. Navy needs for

predicting optical properties arise from the effects these properties have on the performance of various electro-optical surveillance, communications, and weapons systems. Predicted optical properties are input to numerical models, which are used, in turn, to predict electro-optical system performance. Ideally, the optical predictions should be based on ocean color data derived from satellites in near real time. However, due to clouds (and at present, lack of a space-based ocean color system), real-time data will not always be available. The satellite-derived optical climatologies serve two purposes: as a backup to real-time ocean color data and to support planning for operations in a particular region.

The optical property most frequently estimated from ocean color data is $K(490)$, the diffuse attenuation coefficient at a wavelength of 490 nm. The units of $K(490)$ are m^{-1} . A serious limitation of remotely sensed $K(490)$ is that it represents only the upper attenuation length, $1/K(490)$ m, near the sea surface (Gordon and McCluney, 1975). This depth is typically 25 to 35 m in clear, highly oligotrophic waters and is 8 m or less in water over the continental slope and shelf. Absorption by chlorophyll and other plant pigments is a major component of $K(490)$, and variability in pigment concentration dominates variability in $K(490)$ horizontally, vertically, and over time. Because of light adaptation by phytoplankton, the vertical profile of pigment concentration is typically characterized by a "deep chlorophyll maximum," found at depths two to three times deeper than the $1/K(490)$ -m depth viewed by the satellite (Cullen and Eppley, 1981). Because of this characteristic profile, surface optical properties are not directly representative of those over the complete water column of interest (e.g., the top 200 m in the deep ocean). Recent work demonstrated, however, that a limited number of in-water optical profiles can be used to develop empirical regression models to predict complete optical profiles from remotely sensed $K(490)$ on a seasonal and regional basis (Mueller and Lange, 1989). An eventual goal of Navy research is to combine satellite-derived ocean color surface $K(490)$ distributions with regression models to yield a three-dimensional climatology for regional prediction of optical properties globally. Even with real-time ocean color data, the climatology will provide the necessary framework for three-dimensional analysis and prediction.

NASA's Goddard Space Flight Center has constructed a global data base of historical CZCS data (1978–1986). All valid CZCS data were averaged into monthly composites and stored in digital image format at a spatial resolution of 20 km. The data base includes water-leaving radiance at 443, 520, 550, and 670 nm; chlorophyll-like pigment concentration; and diffuse attenuation coefficient $K(490)$ at 490 nm. Monthly variances are also given for each variable in a 20-km cell. This overall data base (level 3), which is approximately 3 Gbytes in size, is organized into eight geographic regions (four in the

Applications of Ocean Color to Naval Warfare

BC 009:91:321

G. Daniel Hickman
Editor

Prepared for:
The Oceanographer of the Navy (OP-096)
Program Element 0603704N

by:
Remote Sensing Branch
Ocean Sensing and Prediction Division
Ocean Science Directorate

Contributors:
Robert A. Arnone, Temple H. Fay,
John M. Harding, G. Daniel Hickman,
David Lapota, Paul Martin,
James L. Mueller, David K. Young

May 1992

Naval Oceanographic and Atmospheric Research Laboratory
Stennis Space Center, Mississippi 39529-5004

Robert A. Arnone
Advanced Sensor and Survey Branch
Mapping, Charting, and Geodesy Division
Ocean Science Directorate

Temple H. Fay
Pattern Analysis Branch
Mapping, Charting, and Geodesy Division
Ocean Science Directorate

John M. Harding
Ocean Hydrodynamics/Thermodynamics Branch
Ocean Sensing and Prediction Division
Ocean Science Directorate

G. Daniel Hickman
Remote Sensing Branch
Ocean Sensing and Prediction Division
Ocean Science Directorate

Paul J. Martin
Ocean Hydrodynamics/Thermodynamics Branch
Ocean Sensing and Prediction Division
Ocean Science Directorate

David K. Young
Biological and Chemical Oceanography Branch
Oceanography Division
Ocean Science Directorate

Naval Ocean Systems Center
San Diego, California
David Lapota

State University of San Diego
San Diego, California
James L. Mueller

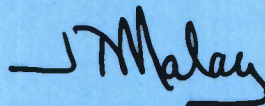
Foreword

This publication is about ocean color; then again, it isn't. Ocean color is precisely what such space-based sensors as the Coastal Zone Color Scanner and the Sea Wide Field-of-View Sensor were designed to observe. But the Navy's interest in ocean color is only because of what ocean color tells us about other properties of the ocean, the medium in which we go to work. Thermal fronts and eddies, biological processes, suspended sediments, and near-shore bathymetry—these properties of the ocean are just some of the by-products of color observations from space. Determining these mission-essential phenomena is why the Navy is interested in ocean color. Computer-enhanced ocean color images are spectacular and marketed as art, but what these images reveal in the art of naval warfare is of far greater value to weapon designers, mission planners, and fleet warfighters.

This is a compilation of the work of several Navy researchers who have investigated the technology and the science behind remote sensing of ocean color. These contributions, collectively as well as individually, are valuable to science and technology purely for the fact that they advance our understanding of this technology. But the real contribution, the one that makes the work worth sponsoring with Navy funding, comes from the *applications* of ocean color—and there are many, as you will find.

The nature of many of these applications make an unclassified discussion impossible, and these applications are not presented here. What will become clear, however, is that acoustic and nonacoustic submarine warfare will receive the greatest benefits from ocean color imaging. In addition to ASW applications, Amphibious Warfare, Special Warfare, and Mine Warfare—all fought primarily in the coastal zone—are supported through ocean color observations of shallow-water conditions. Measurements of optical transmissivity for laser communications assessments and of atmospheric aerosols for electromagnetic and electro-optical propagation predictions are only two examples of how ocean color sensors can also contribute to Space and Electronics Warfare.

Ocean color imaging is not a new science, and the applications discussed here are now becoming well understood. And yet the space oceanography community continues to press on to unlock new secrets of the ocean through color research. The Navy supports these efforts because with each new secret that remote sensing uncovers, we will no doubt be able to apply that secret to the ongoing challenge of naval warfare.



Jonathan T. Malay, Commander, U.S. Navy
Head, Tactical Oceanography Branch
Office of the Oceanographer of the Navy

Summary

Remotely sensed ocean color technology offers the Navy a new source of environmental information to support U.S. Navy warfare operations and planning. Potential naval applications of ocean color were reviewed in a recent workshop report (Pressman et al., 1989). This publication gives examples of ocean color applications that satisfy well-recognized requirements for oceanographic information in naval warfare activities. The technology behind these examples is sufficiently mature to allow near-term development of naval applications to use the new satellite ocean color instrument, the Sea-viewing Wide-Field-of-View Sensor (SeaWiFS), beginning in 1993. Operational implementations of these "naval applications" will be based on real-time satellite ocean color imagery, backed up by optical climatologies derived through offline analyses.

Ocean color is the spectral reflectance of the water column. It is measured remotely as wavelength-dependent radiance emerging from the sea surface. Ratios of water-leaving radiances are used to calculate phytoplankton pigment concentration (Gordon et al., 1983), and optical diffuse attenuation coefficients (Austin and Petzold, 1981; Mueller et al., 1990). When ocean color is measured from space using images composed of visible wavelengths, up to 85% of the radiance measured in the 0.45 to 0.55 μm region is sunlight that is scattered backward by the earth's atmosphere. The atmosphere also attenuates the water-leaving radiance transmitted from the ocean surface on its path to the sensor. Therefore, atmospheric corrections must be applied to derive accurate ocean color parameters from satellite radiance measurements (Gordon et al., 1983; Gordon et al., 1988). Robust methods for removing atmospheric effects and determining ocean bio-optical properties from ocean color imagery have evolved through a decade of research using the Coastal Zone Color Scanner (CZCS) on board the Nimbus-7 earth-orbiting satellite.

The CZCS was a multispectral, imaging radiometer placed in operation on Nimbus-7 in October 1978. This instrument was designed to measure subtle variations in ocean color in four narrow wavelength bands. Its special features included finer spectral resolution, better radiometric sensitivity, and higher signal-to-noise ratios than previous satellite radiometers. The CZCS scan view could also be tilted backward or forward along the subsatellite track to avoid sunglint contamination. The CZCS was turned on several times daily

for brief periods (up to 120 minutes a day) and continued successful operation through mid-1986, a span far longer than its 1-year design life. Researchers are currently attempting to exploit this rich data set for numerous applications, including those of major interest to the U.S. Navy.

Research using CZCS data established the feasibility of using ocean color observations from space to study global and mesoscale distributions of ocean bio-optical properties. NASA recently signed a contract to develop and fly a second-generation satellite ocean color imaging system (SeaWiFS). The SeaWiFS ocean color instrument is designed with eight channels in the visible and near-infrared regions of the electromagnetic spectrum. Four of the visible SeaWiFS channels are similar to those of the CZCS. SeaWiFS will operate globally on a 100% daylight duty cycle, which makes it suitable for the Navy and other realtime operational users, as well as for post processing analyses.

Subject to user fees, the Navy's existing Advanced Very High Resolution Radiometer High Resolution Picture Transmission (HRPT) communications units (SMQ-11 or its successor) will be capable of receiving the SeaWiFS data with only minor modifications. Furthermore, the Navy's Tactical Environmental Satellite System 3 (TESS-3) computer systems will readily handle naval applications analyses of satellite ocean color image data. SeaWiFS will give the Navy a highly cost-effective way to obtain valuable environmental information (compared to developing a dedicated sensor system).

The section on "Optical Climatologies" gives examples of satellite-derived ocean color images that have been shown to yield global information on the visibility of the ocean. This information is valuable for predicting the performance of various naval electro-optical applications, such as aircraft- or satellite-to-submarine communications, and performance predictions applicable to a variety of detectors and/or imaging electro-optical systems in nonacoustic antisubmarine warfare, mine warfare, and bathymetric mapping (see sections on "Coastal Optics" and "Ocean Color Effects on the Operation of Active and Passive Optical Aircraft/Satellite Systems").

"Ocean Color Visualization of Mesoscale Water-Mass Features" previews examples of ocean color. These examples clearly identify mesoscale ocean fronts and eddy features (critical to acoustic predictions for antisubmarine warfare) that are similar to those derived from sea surface temperature. In some cases, however, mesoscale features exist but lack sea surface thermal signatures. These features, when resulting from changes in chlorophyll concentration or turbidity variations, can be observed with ocean color sensors.

Ocean color can be valuable in those locations where the atmosphere is so humid that the infrared derived sea surface temperature measurements are

useless due to strong absorptions of the infrared by the water vapor. Mesoscale features have been observed via ocean color in areas where the changes in the chlorophyll levels are mainly caused by salinity and not temperature gradients. Such features would go undetected using only sea surface temperatures.

“Sensitivity of the Prediction of Upper-Ocean Thermal Structure to Turbidity Estimated from Ocean Color” illustrates that variations in seawater turbidity detected via ocean color can affect the ocean thermal structure on seasonal time scales. Thermal structure changes can result in significant variability in the acoustics at strong water mass boundaries, which in turn can affect sea surface temperature, mixed-layer depth, and acoustic detection range.

Although the majority of the research effort on the use of ocean color for naval applications has been involved with deep-water oceanography using CZCS data, examples derived from both aircraft and satellite sensors show (see “Coastal Optics”) ocean color extended into shallow water. Once appropriate algorithms are developed for (including validations) shallow water, many naval applications (e.g., Mine Warfare, Amphibious Warfare, and Hydrographic Bathymetric Surveying) can greatly profit from the optical sensors.

The examples given in this report show that aircraft and satellite ocean color derived products can be used in conjunction with other remote sensor and *in situ* data to solve major naval requirements. Ocean color has matured to the state where many ocean color products are in various stages of development and transitioning to the U.S. Fleet. However, substantial resources—from basic research through advanced development—should be directed towards ocean color. This support is necessary if the Navy is to fully utilize the potential of this new technology for Naval applications.

Acknowledgments

This report was funded by the Oceanographer of the Navy, under the program management of Lt. Commander W. A. Cook (Program Element 0603704N), Space and Naval Warfare Systems Command, Satellite Applications and Techniques Program. The work was performed under the leadership of Mr. A. E. Pressman, Head of the Remote Sensing Branch at the Naval Oceanographic and Atmospheric Research Laboratory.

Special appreciation is extended to Mr. Don Montgomery, Dr. A. W. Green, Jr., and Dr. M. J. Duggin for reading this document and giving their constructive criticism.

Contents

Foreword	i
Summary	iii
Acknowledgments	vi
I. Optical Climatologies	1
<i>Robert A. Arnone and James L. Mueller</i>	
II. Ocean Color Visualization of Mesoscale Water Mass Features	7
<i>James L. Mueller, Robert A. Arnone, and John M. Harding</i>	
III. Sensitivity of the Prediction of Upper-Ocean Thermal Structure to Turbidity Estimated from Ocean Color	18
<i>Paul Martin, John M. Harding, James L. Mueller, and Robert A. Arnone</i>	
IV. Coastal Optics	25
<i>G. Daniel Hickman, Robert A. Arnone, and Temple H. Fay</i>	
V. Ocean Color Effects on the Operation of Active and Passive Optical Aircraft/Satellite Systems	32
<i>David K. Young, David Lapota, and G. Daniel Hickman</i>	
VI. References	39

Optical Climatologies

Abstract: Satellite-derived ocean color data yield global information on optical properties of the ocean. This information is important in predicting the performance of various Navy electro-optical systems. Although optical climatologies are valuable for planning various Navy applications, real-time, satellite-derived, ocean optical parameters are paramount to the effective operation of many weapon systems.

Significant advances in optical oceanography have recently been made by using satellite-derived ocean color data. The Coastal Zone Color Scanner (CZCS) data base provided the first global overview of the spatial and temporal distributions of near-surface bio-optical properties (Austin and Petzold, 1981; Smith and Baker, 1978, 1982; Gordon et al., 1980, 1983) and scales of variability. In deep-ocean Case I waters, where the concentration of phytoplankton is high compared to that of other particles (Morel and Prieur, 1977), optical properties vary seasonally and co-vary with surface phytoplankton concentrations.

In open-ocean frontal areas and in coastal waters, satellite ocean color data reveal a more spatially complex and temporally variable structure than had been envisioned. The academic research community is aggressively pursuing research to use the spatial and temporal information in global ocean color climatologies. This information will allow global primary productivity and related processes that control the carbon-dioxide and other biogeochemical cycles in the ocean-atmosphere-terrestrial system to be better quantified and understood. Ocean color data from the forthcoming SeaWiFS figure prominently in planning for Joint Global Ocean Flux Study (JGOFS) research over the coming decade.

For many Navy applications, ocean color climatologies based on the CZCS (and the SeaWiFS) data provide estimates of regional ocean optical properties and of variability on mesoscale, seasonal, and regional scales. Navy needs for

predicting optical properties arise from the effects these properties have on the performance of various electro-optical surveillance, communications, and weapons systems. Predicted optical properties are input to numerical models, which are used, in turn, to predict electro-optical system performance. Ideally, the optical predictions should be based on ocean color data derived from satellites in near real time. However, due to clouds (and at present, lack of a space-based ocean color system), real-time data will not always be available. The satellite-derived optical climatologies serve two purposes: as a backup to real-time ocean color data and to support planning for operations in a particular region.

The optical property most frequently estimated from ocean color data is $K(490)$, the diffuse attenuation coefficient at a wavelength of 490 nm. The units of $K(490)$ are m^{-1} . A serious limitation of remotely sensed $K(490)$ is that it represents only the upper attenuation length, $1/K(490)$ m, near the sea surface (Gordon and McCluney, 1975). This depth is typically 25 to 35 m in clear, highly oligotrophic waters and is 8 m or less in water over the continental slope and shelf. Absorption by chlorophyll and other plant pigments is a major component of $K(490)$, and variability in pigment concentration dominates variability in $K(490)$ horizontally, vertically, and over time. Because of light adaptation by phytoplankton, the vertical profile of pigment concentration is typically characterized by a "deep chlorophyll maximum," found at depths two to three times deeper than the $1/K(490)$ -m depth viewed by the satellite (Cullen and Eppley, 1981). Because of this characteristic profile, surface optical properties are not directly representative of those over the complete water column of interest (e.g., the top 200 m in the deep ocean). Recent work demonstrated, however, that a limited number of in-water optical profiles can be used to develop empirical regression models to predict complete optical profiles from remotely sensed $K(490)$ on a seasonal and regional basis (Mueller and Lange, 1989). An eventual goal of Navy research is to combine satellite-derived ocean color surface $K(490)$ distributions with regression models to yield a three-dimensional climatology for regional prediction of optical properties globally. Even with real-time ocean color data, the climatology will provide the necessary framework for three-dimensional analysis and prediction.

NASA's Goddard Space Flight Center has constructed a global data base of historical CZCS data (1978–1986). All valid CZCS data were averaged into monthly composites and stored in digital image format at a spatial resolution of 20 km. The data base includes water-leaving radiance at 443, 520, 550, and 670 nm; chlorophyll-like pigment concentration; and diffuse attenuation coefficient $K(490)$ at 490 nm. Monthly variances are also given for each variable in a 20-km cell. This overall data base (level 3), which is approximately 3 Gbytes in size, is organized into eight geographic regions (four in the

Northern Hemisphere and four in the Southern Hemisphere). This data base is on line and is available for immediate product retrievals in support of Navy operations.

Figure 1 is an example of part of the optical data base for April 1979 in the North Atlantic (region 2). The figure represents mean surface diffuse attenuation coefficients $K(490)$ measured for a 512×512 square pixel area (20-km pixel resolution). All CZCS processing was performed using the SeaPac image processing system (Firestone et al., 1989). In this image of the North Atlantic, the elevated surface $K(490)$ values (red) arise from high phytoplankton pigment concentrations produced by the spring bloom. Correspondingly, the low $K(490)$ values are characteristic of the Sargasso Sea region (blue). The overall distribution of the optical properties in the image is closely associated with the general anticyclonic oceanic circulation in the North Atlantic. Moreover, the 20-km resolution of this data base has sufficient detail to identify a cold-core eddy (green) south of the Gulf Stream and southeast of Cape Hatteras. However, many individual meander patterns and eddy features associated with the Gulf Stream appear disjointed and blurred because this figure represents "composite-averaged" conditions over a full month.

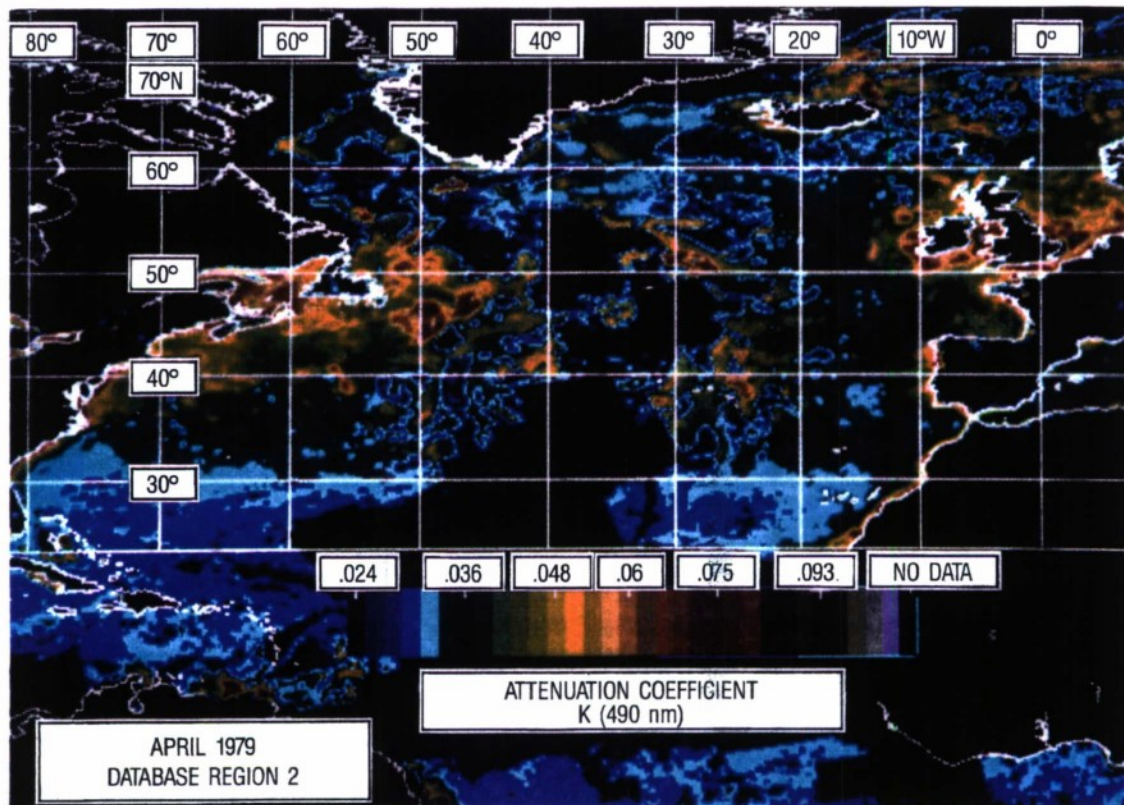


Figure 1. The average diffuse attenuation coefficient, $K(490)$, derived from the Coastal Zone Color Scanner (CZCS) for April 1979. Black indicates cloud cover or lack of satellite coverage.

The CZCS climatology can provide environmental information for naval planning in regions where in-water optical measurements are difficult to obtain. Figure 2 is an enlargement of the mean monthly K(490) data base illustrating the Arabian Sea and the Persian Gulf. This image represents the September 1979 composite average of optical properties. The Somali Current is observed as elevated K(490) values moving north along the Somali Coast and then turning eastward into the Arabian Sea (Oriol and Arnone, 1990). An anticyclonic oligotrophic gyre is observed in the Gulf of Aden. The gyre appears to remain constant relative to other monthly images. High K(490) values are observed in the Persian Gulf and particularly in the northern region at the discharge of the Shattel Arab River. The 20-km resolution data base provides an initial estimate of the optical properties associated with the circulation and water mass distribution in the area.

In addition to mean K(490) data, the data base contains the standard deviation (not shown) of the K(490) values for the 20-km resolution cells. A standard deviation image represents the stability and dynamics of the optical properties. High standard deviations signify that the optical properties changed during the month either as a result of growth or decay (or both) of the phytoplankton population or because differing water masses advected into the region. Spatial variability within individual 20-km cells also contributes to high standard

deviation in these areas. Therefore, such dynamic ocean areas as the frontal position of the Gulf Stream north wall, near-shore coastal waters, and the Grand Banks have high standard deviations. However, standard deviations are uniformly low in the Sargasso Sea. Complex circulation patterns associated with the meanders and eddies, such as exist in the Gulf Stream extension, are retained even in monthly averages over 20-km cells.

Climatology requires that the optical properties over several years be established to characterize the longer times of variability. The interannual mean K(490) variability for the western Pacific and the Gulf of Mexico (region 1) is illustrated for December 1978, 1979, and 1980 (Fig. 3). For example in the Gulf of California, typical K(490) values

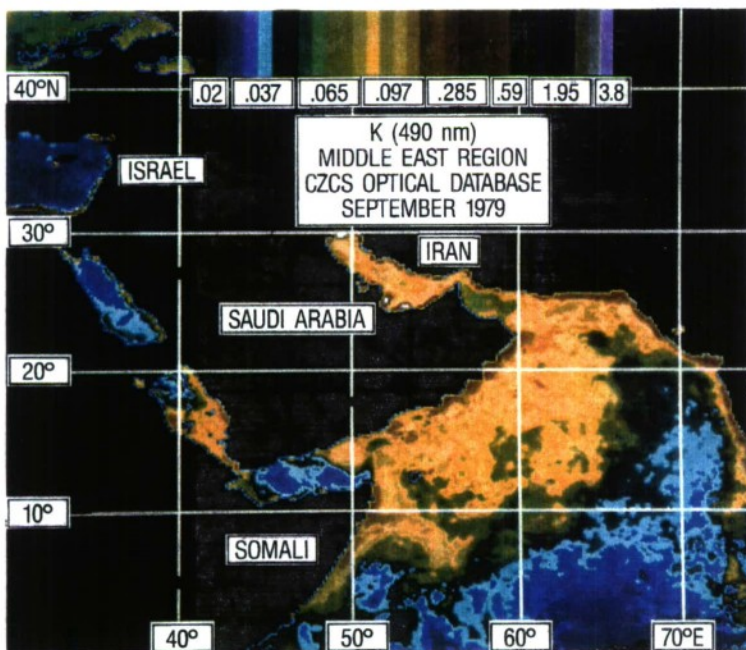


Figure 2. The K(490) data base shown for the Persian Gulf, Eastern Mediterranean, and the Arabian Sea. This image (September 1979) is the start of the monsoon season. The large values for K in the Persian Gulf are closely related to the surface circulation.

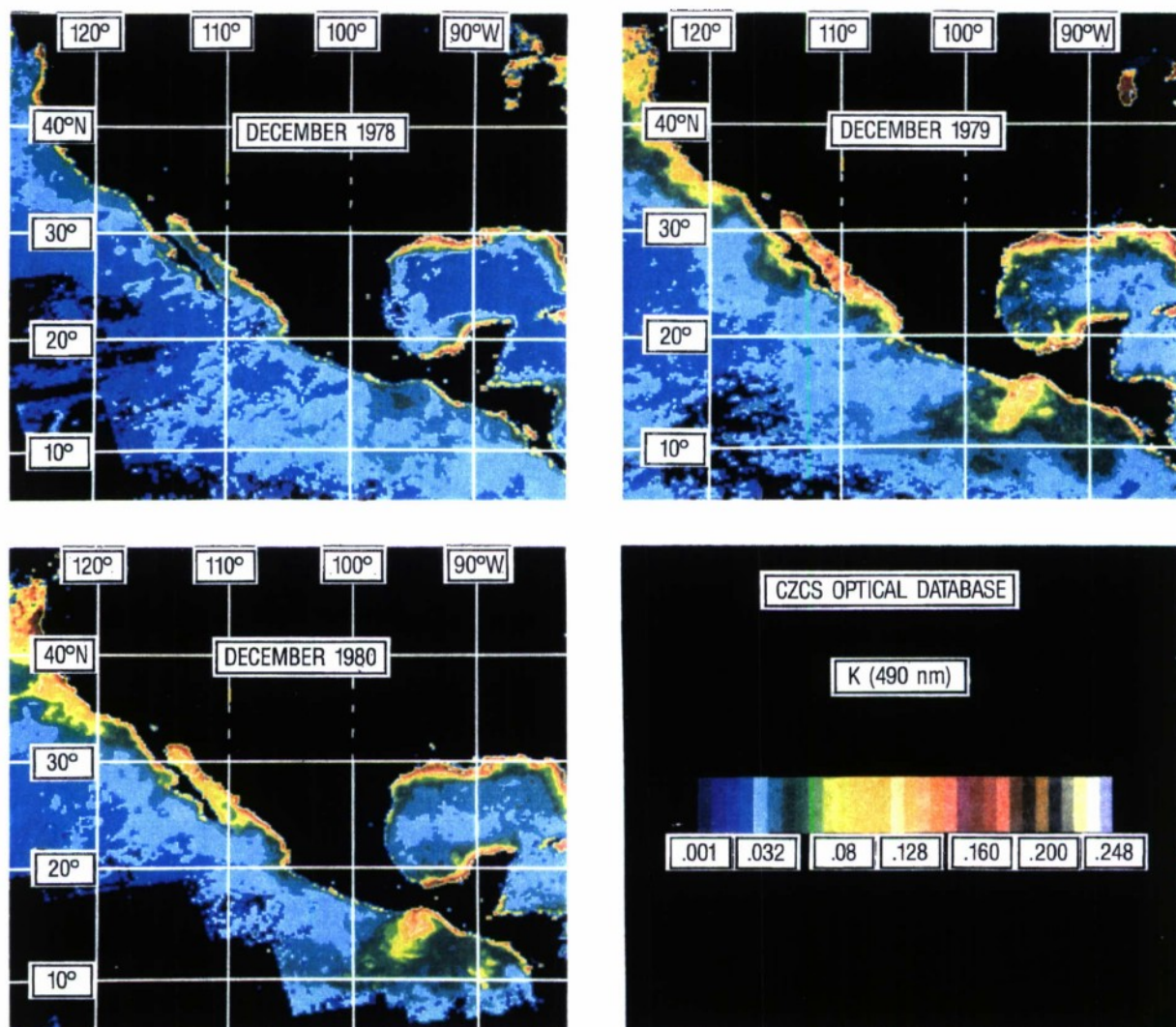


Figure 3. Interannual optical variability of surface waters in the Western Pacific and Gulf of Mexico for December 1978, 1979 and 1980. Similarities and differences in their optical climates can be noted. Note the Gulf of Tujaunipek in Central America.

are lower in 1978 than in 1979 or 1980. However, elevated $K(490)$ values prevail for all 3 years in the Gulf of Tujuanipek (west coast of Central America). Regional estimates of interannual variability provide critical guidance as to when climatology predictions of optical properties are likely to be valid or invalid.

This historical data base from CZCS is a valuable initial attempt to characterize the optical climatology of the world's oceans. Methods for conveniently assessing this optical data base are being developed. Software is available to retrieve yearly $K(490)$ values from the data base using a simple IBM PC program.

James L. Mueller

Robert A. Arnone

John M. Harding

Ocean Color Visualization of Mesoscale Water Mass Features

Abstract: Satellite ocean color imagery that support various warfare areas can be used to enhance water mass differentiation. Ocean color imagery can be substituted for or, in many cases, used to complement infrared sea surface temperatures. Ocean color is particularly valuable when temperatures and atmospheric humidity are high. Under these conditions, surface features appear weak in the infrared image. Sound velocity profiles can also be derived from ocean color data in a manner similar to that using sea surface temperature.

The U.S. Navy has long-standing requirements for water-mass differentiation to support several programs: Antisubmarine Warfare, Sea-based Strategic Warfare, Antisurface Ship Warfare, Mine Warfare, Ocean Surveillance, and Logistics. Each of these naval warfare areas requires knowledge of ocean thermal structure, which can be inferred from water mass identifications based on remotely sensed infrared sea surface temperatures and ocean color imagery.

Today, the Navy uses water-mass differentiation as an operational tool. Maps of ocean fronts and eddies are created at the U.S. Naval Oceanographic Office using all available in situ and remotely sensed data. These maps are then sent by message to ashore sites and afloat units to aid in optimal deployment of air and sea assets to perform the Navy's ASW mission. The front and eddy maps are also sent to the Fleet Numerical Oceanography Center, where they are routinely input into three-dimensional nowcasts of temperature and salinity. These nowcasts are accessed by the Navy's regional oceanography centers, where they are used to calculate range-dependent acoustic propagation forecasts for the U.S. Fleet.

Figure 4a shows the Fleet Numerical Oceanography Center's Gulf Stream sea surface temperature nowcast for 30 April 1990. The realistic gradients across the Gulf Stream and the warm and cold eddies were produced based on satellite infrared sea surface temperature data. At the locations of these

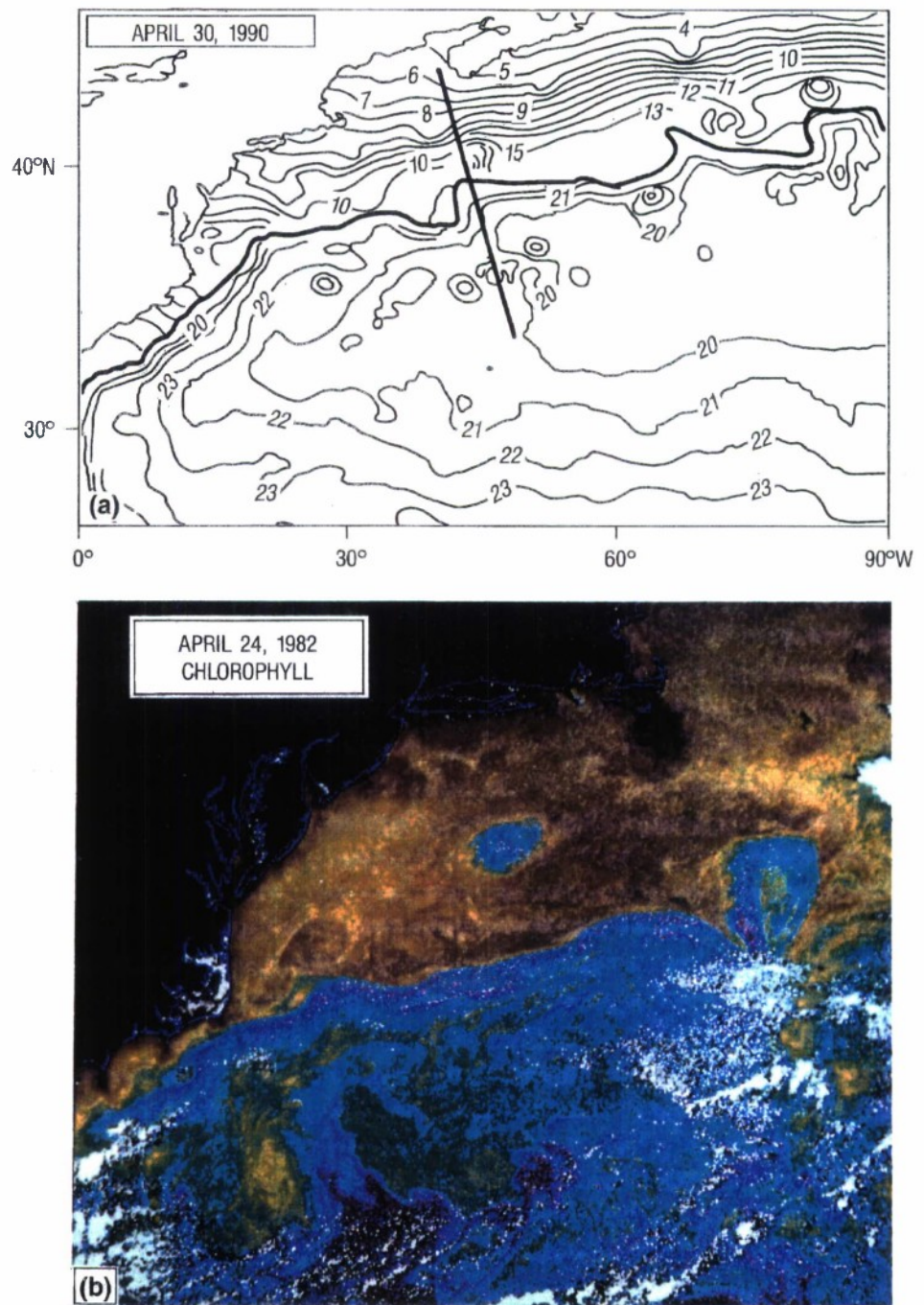


Figure 4. Comparison of Gulf Stream region observed from the CZCS and that produced by FNOc temperature nowcasts. (a) FNOc sea surface temperature nowcast for 1200 Hz, 30 April 1990. The heavy black curve is the nowcast position of the Gulf Stream front, and (b) CZCS derived chlorophyll concentration (C). Low to high values of C are coded as purple-blue-green-yellow-brown-red. Warm core ring 82B is the low chlorophyll feature in the center of the image, 24 April 1982.

water-mass features, “feature models” are used to extend realistic subsurface depictions of the three-dimensional front or eddy structure into the water column. These feature models are based on climatologies of the temperature and salinity characteristics of the water masses that make up these distinct features, with the location and extent of each water mass determined from the sea surface temperature nowcast. The complex, gradient-rich structures of the modeled temperature, salinity, and sound speed, are found to be much more realistic (not shown) than the corresponding sections derived from the Generalized Digital Environmental Model (GDEM) climatology alone (not shown). The GDEM climatology is used by the Navy as a fallback in the Gulf Stream region and exclusively elsewhere in the world where feature models have not been developed.

We will give examples of how ocean color imagery can also be used to identify and locate such water-mass features as fronts and eddies, which are major requirements for Antisubmarine Warfare. In certain situations ocean color has a unique capability to characterize ocean features that is superior to using sea surface temperature. Conditions where sea surface temperature signatures may be either nonexistent or difficult to detect, chlorophyll levels observed via ocean color may still be visible and used to discriminate water masses. This situation can arise during several situations:

- when uniform heating of a shallow surface layer eliminates the sea surface temperature anomaly associated with an eddy, which nevertheless retains its deeper structure;
- when the atmosphere is so humid that absorption by water vapor renders it opaque to infrared radiation, and thus obscures the surface from the view of infrared instruments in space; and
- when the mesoscale ocean feature in question is produced by gradients in salinity, with little associated variation in temperature.

The following text contains examples of cases where ocean color provided the only way to identify mesoscale water-mass features, as well as cases where the features were identified in both infrared sea surface temperatures and ocean color.

Gulf Stream Warm Core Rings and Sound Speed Predictions

As noted, ocean color imagery can be either substituted for or used to complement infrared sea surface temperatures in producing Gulf Stream surface nowcasts (similar to Fig. 4a), and in three-dimensional temperature, salinity, and sound speed analyses. Figure 4b is a map of chlorophyll concentration derived from a Coastal Zone Color Scanner (CZCS) image of the Gulf Stream region on

24 April 1982. The purple and blue shades in the color scale denote optically clear, low-chlorophyll areas; greens to yellows to reds denote progressively increasing concentrations (or decreasing water transparency). The light-blue, low-chlorophyll feature in the center of the image (due east of Delaware Bay and south of the eastern tip of Long Island) is warm-core ring 82B (the second warm-core ring formed in 1982). Schmitt and Olson (1985) report results of a shipboard conductivity-temperature-depth section through warm-core ring 82B during April 1982. The temperature distribution and salinity results were similar to those in the warm-core ring sighted just north of the Gulf Stream wall in the 30 April 1990 nowcast in Figure 4a. In this case, the front and eddy features in the ocean color image for 24 April 1982 (Fig. 4b) could have been used in place of the sea surface temperatures to generate front and eddy nowcasts and three-dimensional temperature, sound speed, and salinity maps (Fig. 5).

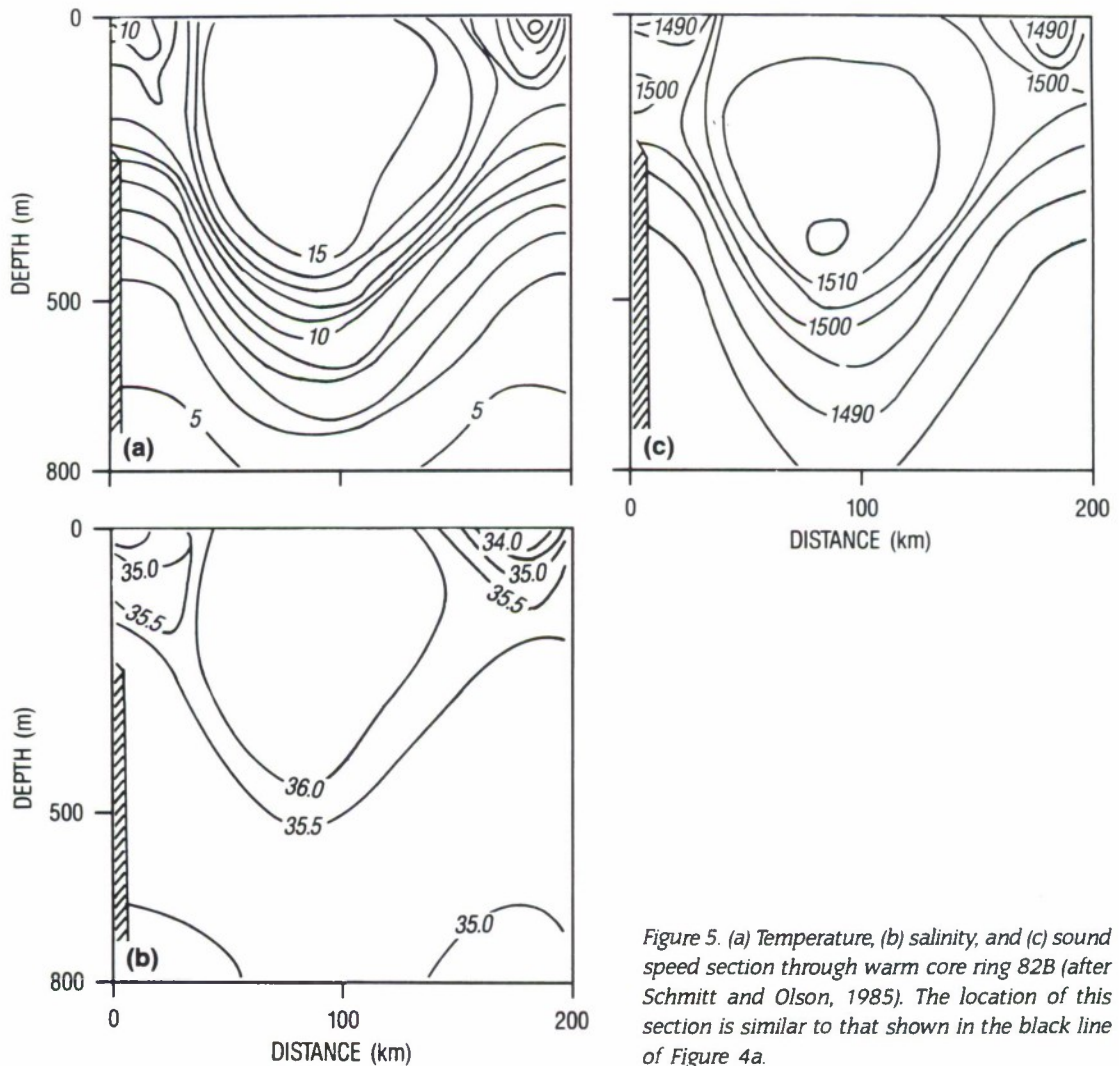


Figure 5. (a) Temperature, (b) salinity, and (c) sound speed section through warm core ring 82B (after Schmitt and Olson, 1985). The location of this section is similar to that shown in the black line of Figure 4a.

The U.S. Navy uses surface fronts and eddy nowcasts in their operational analyses, but does not use feature models for acoustic forecasts in the California current region. The Navy also relies on the GDEM climatology, which predicts greatly smoothed sound speed fields with unrealistically weak gradients. It is feasible to develop feature models based on well-known temperature and salinity characteristics of California current water masses. Furthermore, ocean color images can be used to delineate the locations and extent of acoustically important water-mass features. (The same holds true for sea surface temperatures, and both data types should be exploited for this application.) The pathway to improved operational acoustic predictions in the eastern North Pacific Ocean is a straightforward extension of the front and eddy nowcasting (using SeaWiFS¹ color data, AVHRR² infrared sea surface temperature data, and in situ temperature profiles), and three-dimensional feature-modeling techniques, which are presently used only in the Gulf Stream region.

Gulf of Mexico Loop Current and Eddies: Comparison of Ocean Color and Sea Surface Temperature

In the examples described in the preceding text, ocean color and infrared sea surface temperature imagery would yield roughly equivalent information on the location and size of water-mass features. However, the situation can be quite different at low latitudes during the summer. Intense heating of a shallow surface layer tends to reduce, or even eliminate, the surface temperature contrast between different water masses at the shallow skin depth sensed in the infrared. Therefore, fronts and eddies appear as weak features, if they appear at all, in the infrared sea surface temperature field. The problem is compounded further because atmospheric humidity often becomes extremely high at these latitudes—to the point that absorption by water vapor may render the atmosphere virtually opaque at infrared wavelengths. The net result of these phenomena is that mesoscale water-mass features are invisible in infrared sea surface temperature imagery observed under these conditions.

The contrast in ocean color among water-mass features is derived primarily from differing concentrations of phytoplankton pigment in the uppermost optical depth of the water column. At visible wavelengths used for remote sensing of ocean color, this depth ranges from 2.5 m to 3 m in extremely turbid water masses, to as much as 40 m in the clearest ocean waters. The optical properties in this part of the water column are not generally affected by surface heating; therefore, any contrast in ocean color among water masses may persist throughout the summer.

¹ Sea-viewing Wide-Field-of-View Sensor

² Advanced Very High Resolution Radiometer

Furthermore, water vapor is almost completely transparent to radiation at visible wavelengths, so features not seen by

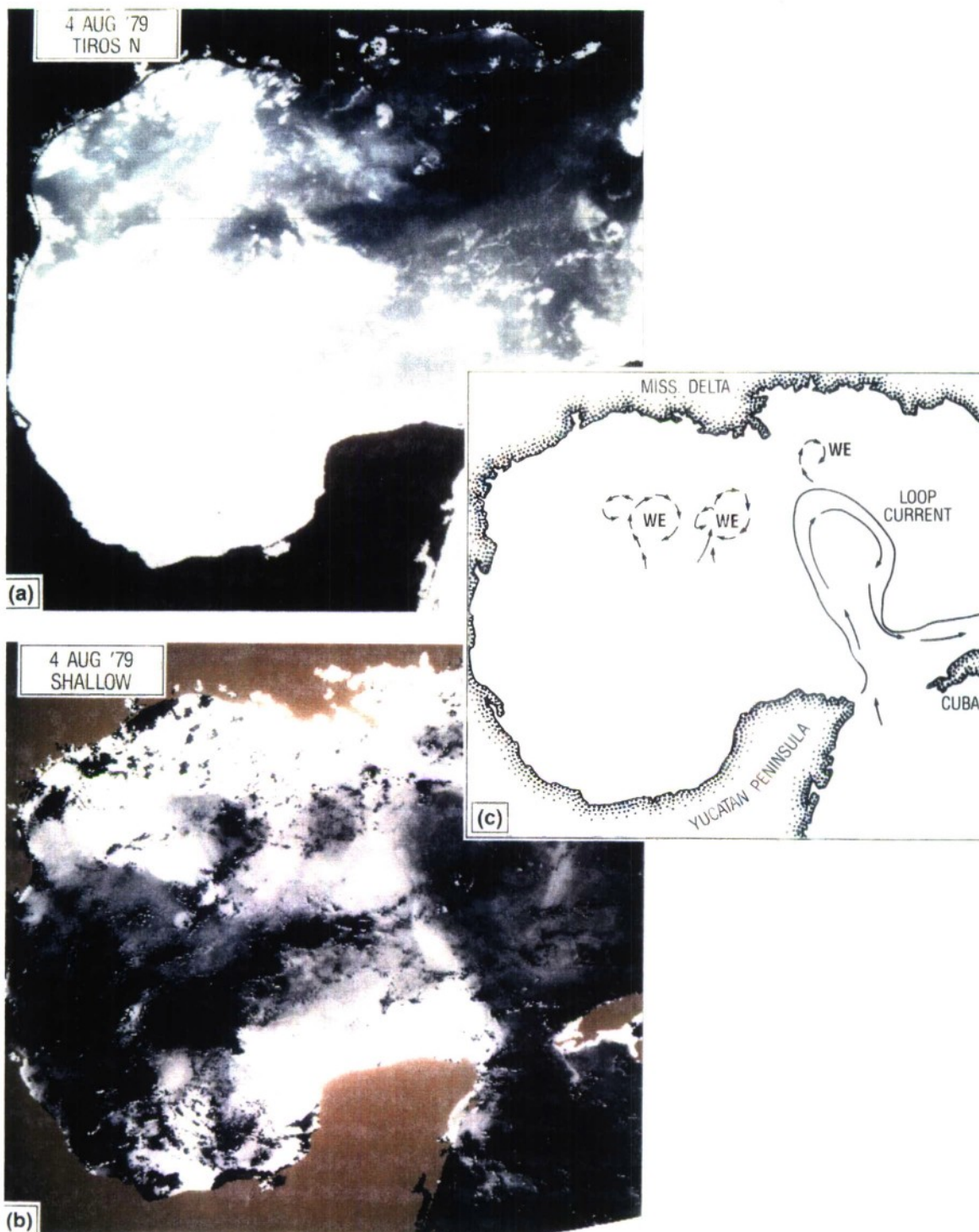


Figure 6. Comparison of infrared image taken with the AVHRR and the CZCS of the Gulf of Mexico. (a) Tiros-N infrared image of the Gulf of Mexico (4 August 1979). High concentrations of atmospheric water vapor obscure the surface temperature field from view. (b) CZCS ocean color image of Gulf of Mexico (4 August 1979). Mesoscale water mass features visualized in this image include the Loop current and several warm eddies. These features are not seen in the infrared image (a). (c) Qualitative circulation the Loop current and warm eddies (marked "WE") as interpreted from the CZCS image (b).

infrared sea surface temperature imagery can remain distinctly visible in ocean color imagery.

Figure 6a is an example of this type of situation. This figure is an infrared image of the Gulf of Mexico taken with the AVHRR on board the Tiros-N satellite on 4 August 1979. Dark-gray shades are warm, and light shades are cold. Virtually the only structure seen in this image is due to clouds and atmospheric water vapor, and there is little or no information about the underlying features of ocean circulation. However, the CZCS image from 4 August 1979 (Fig. 6b) shows several mesoscale and large-scale features of the circulation in the Gulf of Mexico. A qualitative description of the flow associated with these features is shown schematically in Fig. 6c. The warm, low-chlorophyll (dark-gray shades) Loop Current flows northward into the central Gulf of Mexico, with its western boundary traced by high-chlorophyll (light-gray shades) waters entrained off the Yucatan Peninsula (Fig. 6b). Other prominent features can be seen in the ocean color data, but not in the infrared sea surface temperature data, include two warm eddy (WE) doublets in the western Gulf of Mexico.

The physical oceanography of the water masses of the Gulf of Mexico is well enough known to implement operational water-mass feature analyses and models, which are similar to those used to produce three-dimensional sound speed fields for the Gulf Stream region. As shown by the present example, however, satellite ocean color imagery is essential to water-mass feature nowcasting in this region, since infrared sea surface temperature imagery is not useful here during the summer.

The Alboran Gyre and Algerian Current: Ocean Color and Sea Surface Temperature Interpretations

Several ocean circulation features in the western Mediterranean Sea illustrate the relative merits of using remotely sensed ocean color and sea surface temperature for detecting ocean fronts and water-mass features. Figure 7a is the AVHRR infrared sea surface temperature image, which was taken during the daytime pass of the NOAA-9 satellite over the western Mediterranean Sea. Light-gray shades are cold-water temperatures, and dark-gray shades are warm-water temperatures. Winds were light on this date, and solar heating of a shallow surface layer obscured much of the underlying ocean thermal structure in the infrared image. For example, the patch of warm water to the south and the west of Mallorca manifests diurnal heating of a very shallow surface layer. This patch has no relationship to the underlying water-mass structure in the area as seen by the CZCS image of phytoplankton pigment concentration taken on the same day (Fig. 7b). The water-mass and flow patterns associated with

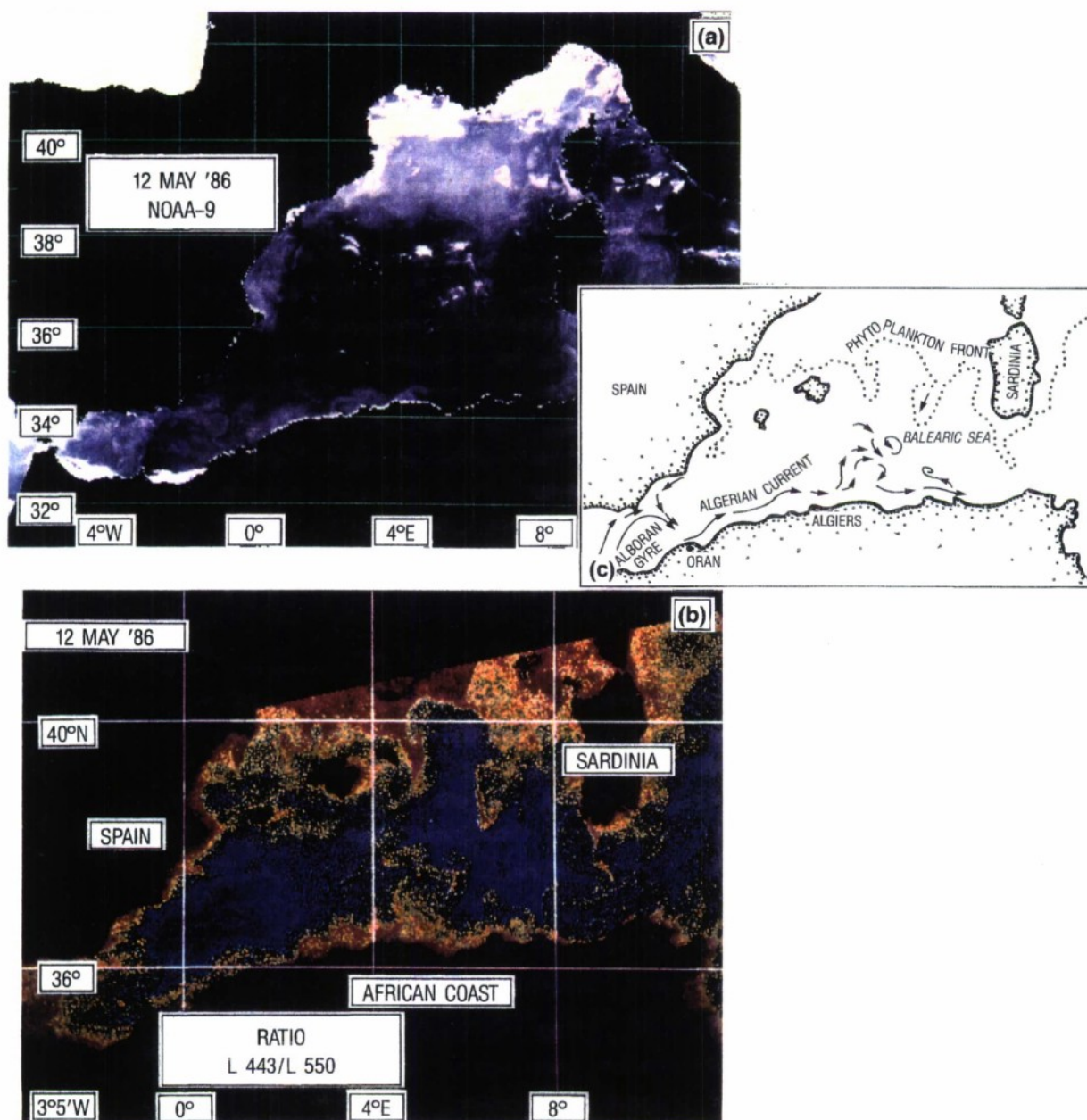


Figure 7. Circulation patterns in the Western Mediterranean Sea derived from SSTs (AVHRR) and pigment concentrations from CZCS – 12 May 1986. (a) Infrared sea surface temperature measured by the AVHRR during the daytime pass of the NOAA-9 satellite. Dark shades represent warm temperatures and light shades cold temperatures. (b) CZCS pigment concentrations. Low to high chlorophyll concentration are color coded as blue-green-yellow-orange-brown. (c) Schematic diagram of mesoscale features as interpreted from CZCS ocean color and AVHRR sea surface temperature.

the Alboran Gyre and Algerian Current, as inferred from these images, is shown schematically in Figure 7c. Contrast the well-defined structure of the phytoplankton front with the relatively weak sea surface temperature gradients associated with this water-mass boundary in the infrared image. Compare also the circulation features along the north coast of Africa associated with the Algerian Current; many of the eddies associated with the Algerian Current are clearly visible in the ocean color image but are not seen at all in the infrared image.

The ocean color contrast associated with the elevated phytoplankton concentration in this salinity-driven current provides a better tracer of the feature than does infrared sea surface temperature.

The Alboran Sea: Temperature/Color Water-Mass Classification

The previous examples demonstrated that ocean color imagery can now be used either as well as or, in some instances, to better advantage than infrared sea surface temperature imagery to determine the location, shape, and size of water-mass features and their associated frontal boundaries. Arnone (1987) established that water masses can be classified and identified on the basis of the joint surface temperature and phytoplankton pigment concentration. He used a method analogous to that used with temperature and salinity diagrams to trace deep-water masses.

Figure 8 shows the AVHRR infrared sea surface temperature and the CZCS ocean color imagery for 13 October 1982 in the western Mediterranean Sea. Sea surface temperature contours taken from the infrared image are superimposed on the ocean color imagery. The paired temperature and chlorophyll data were used in an unsupervised classification algorithm to associate temperature and chlorophyll values with distinct water masses. The data used to define individual water masses were taken from features with well-known water-mass characteristics, including major fronts, the gyres of the Alboran Sea, oligotrophic waters in the central Mediterranean and North Atlantic, and coastal estuarine discharge plumes. The resultant water-mass classification and temperature/chlorophyll regions were combined to classify the area's water masses into 26 distinct levels (Fig. 9).

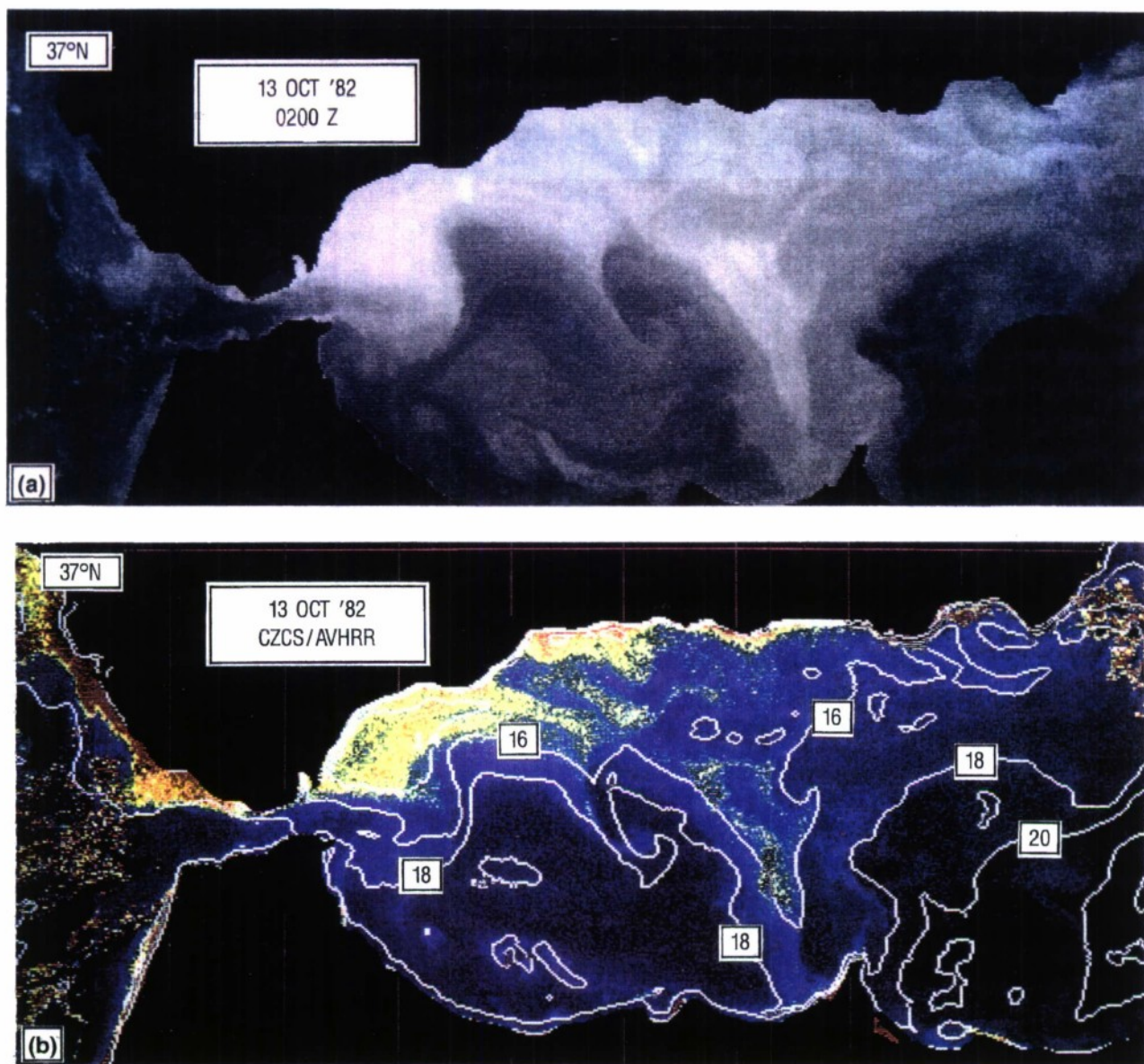
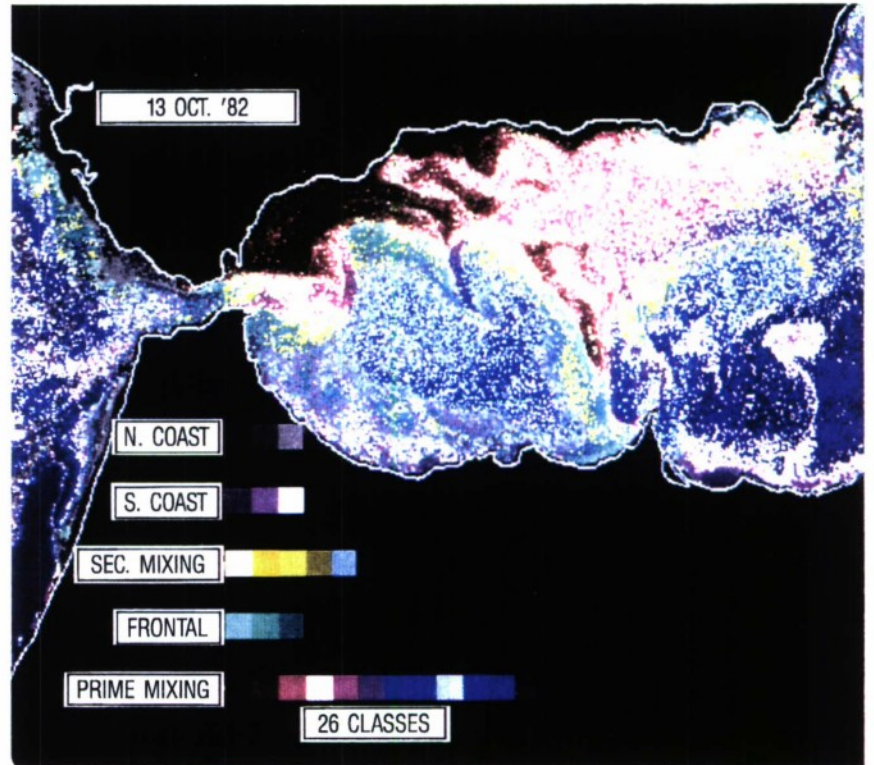


Figure 8. (a) AVHRR sea surface temperature, and (b) CZCS chlorophyll concentration in the Western Mediterranean Sea – 13 October 1982. The images were acquired approximately two hours apart. Temperature contours determined from infrared data are plotted on the ocean color display (Arnone, 1987).

Figure 9. Water mass distribution in the Mediterranean Sea on 13 October 1982, based on temperature/chlorophyll classification (Arnone, 1987).



Paul Martin

John M. Harding

James L. Mueller

Robert A. Arnone

Sensitivity of the Prediction of Upper-Ocean Thermal Structure to Turbidity Estimated from Ocean Color

Abstract: Variations in seawater turbidity can significantly affect the evolution of upper-ocean thermal structure as predicted by ocean models. On seasonal time scales, this turbidity/thermal structure relationship translates into an important spatial variability in regions with sharp water-mass boundaries, such as the Gulf Stream and the Kuroshio and California current systems. In addition, on relatively short time scales, changes in sea surface temperature, mixed-layer depth, and acoustic propagation caused by atmospheric forcing can be sensitive to seawater turbidity. Therefore, upper-ocean turbidity, which can be globally sensed by space-based ocean color sensors, is directly related to oceanographic parameters that affect acoustic transmission related to shallow-water ducting, which is of prime importance to improved oceanographic models and naval tactical applications.

The optical properties of the upper ocean significantly affect the evolution of the ocean's thermal structure. The thermal structure of the upper ocean evolves on time scales ranging from hours to years due to atmospheric fluxes, mixing, and advective processes. Both the heating and the mixing of the upper ocean can be strongly affected by the depth that solar radiation penetrates below the surface. This penetration depth is dependent on the optical clarity of the water.

When solar radiation penetrates the ocean, heating and mixing are affected in several ways. Penetration below the mixed layer during the heating season in both spring and summer directly warms the seasonal thermocline. Because of this, the seasonal thermocline becomes warmer and the mixed layer becomes cooler than would occur if all the solar radiation were absorbed at or very near the surface. The reduced heating of the mixed layer and

the warming of the region below result in a weaker thermal gradient that is more easily eroded by mixing. Within the mixed layer itself, the penetration of solar radiation reduces the vertical density gradients against which mixing must work. This reduction causes stronger and deeper mixing.

The penetration of solar radiation, coupled with surface heat loss from longwave radiation and latent and sensible heat exchange, generates a negative temperature gradient near the surface that can drive convective mixing, even when these fluxes cause net heating of the ocean. This convection generally limits the shallowing of the mixed layer in the case of strong heating and light winds, and moderates the increase of sea surface temperatures during such events. When the net surface heat flux is positive but is small relative to its solar component when averaged over a particular time (typical of the tropics) and the water is fairly clear, the compensation depth can be tens of meters deep. (The compensation depth is the depth at which the downward penetration of solar radiative flux is equal to the net surface heat flux.) Free convection can mix to this depth if not limited by existing density stratification. In such situations, wind-driven mixing may also be enhanced because of weak vertical density gradients.

Both the penetration and the absorption of visible radiation into the sea are controlled by the vertical profile of the diffuse attenuation coefficient $K(z, \lambda)$, where z is the depth of water and λ is the wavelength. As discussed in the previous article, near-surface $K(490)$ can be estimated from satellite ocean color data. Mueller and Lange (1989) showed that $K(490)$ data taken via satellite can be used with empirical regression models to predict the $K(z, 490)$ profile to much deeper depths, albeit on a seasonal and regional basis. Given $K(z, 490)$, the attenuation profile at other visible wavelengths can be estimated using the empirical model of Austin and Petzold (1986). Through this pathway, satellite ocean color data can be used to calculate vertical extinction profiles for short-wave radiation incident on the sea surface.

This section discusses the sensitivity of mixed-layer thermal and acoustic propagation structure to realistic variations in the vertical extinction profile. Extinction profiles derived from the Jerlov water-type classification are first used to explore the sensitivity of mixed-layer models to different optical profiles, given the incident radiation and atmospheric forcing typically found at Ocean Station November in the northeast Pacific. These calculations allow the effects of optical variability on temperature structure over seasonal time scales to be explored.

The sensitivity of mixed-layer simulations to spatially varying radiation extinction profiles on shorter time scales was investigated. Hindcast experiments

were run using water-mass, radiation, and atmospheric-forcing conditions typical of the California current system, together with optical extinction profiles derived from the combined models of Mueller and Lange (1989) and Austin and Petzold (1986). These hindcasts illuminate short time-scale variability of temperature structure and acoustic detection range in response to changing optical profiles in different months over a single year.

Figure 10a shows the fraction of the total surface solar radiation that penetrates to various depths for several types of ocean water that have been characterized according to their optical properties (Jerlov, 1976). These optical classifications,

designated as types I, IA, IB, II, and III, in order of increasing turbidity, are representative of the different optical water types found in the open ocean (Jerlov defined a separate set of water types for coastal regions). Common to all water types is that over half the solar radiation, primarily the infrared part of the spectrum, is absorbed in the upper meter. However, the shorter wavelengths can penetrate much farther, and there is considerable variability in the penetration depth of the shorter wavelengths with seawater turbidity; e.g., for optical type I seawater, over 5% of the total surface solar radiation penetrates below 50 m, but for type III, less than 0.05% penetrates to this depth.

The sensitivity of mixed-layer simulations to the depth that solar radiation penetrates has been noted by a number of investigators (e.g., Kraus and Turner, 1967; Denman and Miyake, 1973; Alexander and Kim, 1976; Simpson and Dickey, 1981; and Martin, 1985). Figure 11 (Martin, 1985) shows a comparison of isotherm

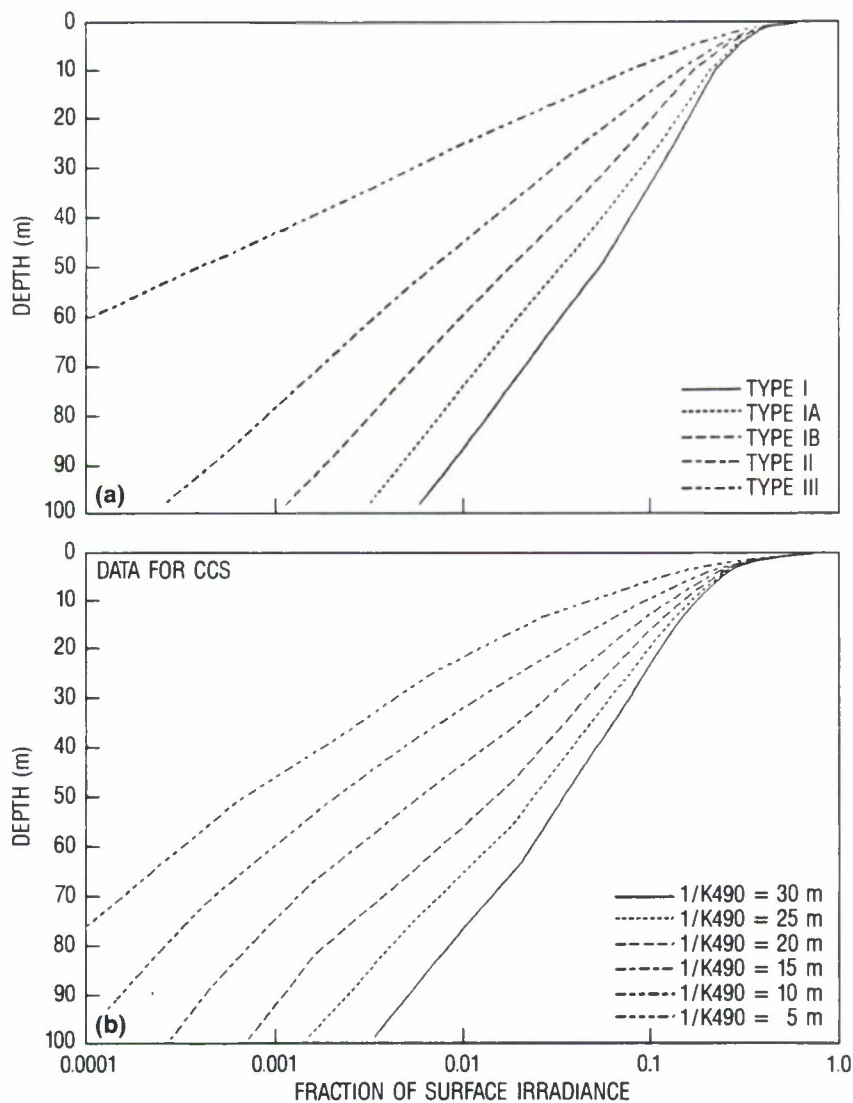


Figure 10. Fraction of total solar radiation that penetrates to various depth of several types of ocean water. (a) Extinction profiles for Jerlov optical water type, and (b) extinction profiles derived from $K(490)$ values.

depths for year-long mixed-layer simulations at Ocean Station November (140°W, 30°N in the northeast Pacific) that were conducted with extinction profiles for Jerlov optical type I (Fig. 11a) and type III (Fig. 11b) seawater. With the higher turbidity, much less heat penetrates below the mixed layer during spring and summer; the mixed layer itself is warmer and shallower, and the seasonal thermocline is nearer the surface and has a much sharper gradient. Rutkovskaya and Khalemskiy (1973) characterize the area around November to be Jerlov type I or IA. Model simulations assuming type I water are in closer agreement with the observed thermal structure than those with type III where warming of the seasonal thermocline is insufficient and sea surface temperatures are too high (Martin, 1985). This comparison illustrates that the erroneous specification of solar extinction in ocean models can lead to large errors in thermal structure and heat storage in long-term integrations.

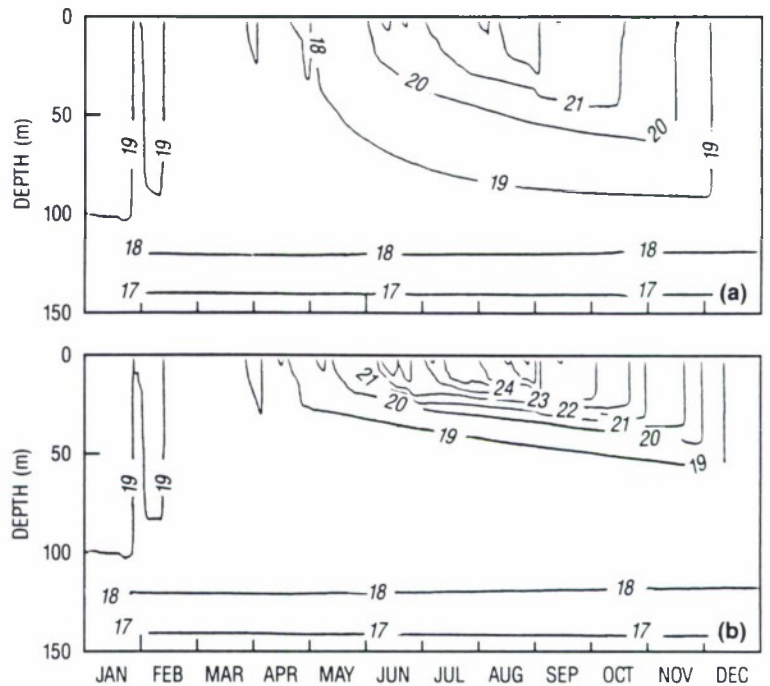


Figure 11. Isotherm depths for year-long mixed-layer simulations at Ocean Station November for 1961 conducted with different seawater turbidities. (a) Calculations using extinction profile for Jerlov optical type I seawater, and (b) calculations using extinction profile for Jerlov optical type III seawater.

A similar comparison for year-long mixed-layer simulations was made for Ocean Station Papa, located 20° north of November at 145°W, 50°N. The effect of the change in the turbidity at Papa was considerably less than at November. The difference was due to the weaker solar radiation and stronger winds at Papa. With less solar radiation, less heat penetrates and directly warms the subsurface water. Stronger winds tend to reduce the frequency and duration of shallow mixed layers that can warm rapidly and generate the stratification inhibiting future deepening. Hence, the sensitivity of upper-ocean thermal structure and mixing to turbidity is likely to be largest where the solar flux is large, the winds are light, and the turbidity variability is high. The variability of turbidity at November, which is located in a large anticyclonic gyre of relatively low biological productivity, is fairly small. However, east of November near the California current system, the spatial and temporal variability of turbidity is relatively high. This high variability is due to the intermingling of clearer waters from the open ocean with biologically productive, nutrient-rich water advected out from the coast. Coastal Zone Color

Scanner (CZCS) images from this region (not shown) indicate high variability in the turbidity. Extinction profiles observed with the CZCS for total solar radiation, based on the surface value of the diffuse attenuation coefficient at 490 nm ($K(490)$), were derived for this and other regions based on in situ turbidity measurements (Mueller and Lange, 1989). Figure 10b shows the fraction of the total solar radiation that penetrated to various depths in the California Current System for different values of $K(490)$. These extinction profiles show a range of variability similar to those for the Jerlov optical types (Fig. 10a).

The ocean color variability observed at Ocean Station November in the California Current System images, combined with the sensitivity to turbidity, demonstrated the potential for both seasonal and spatial sensitivity of upper-ocean thermal structure to seawater turbidity in this current system. We might also expect sensitivity to turbidity of upper-ocean thermal structure for regions near western boundary currents, such as the Gulf Stream and the Kuroshio, that occur at comparable latitudes and display similar high spatial and temporal variability of ocean color.

The sensitivity of short-time-scale, mixed-layer-model hindcasts to the variability of seawater turbidity observed in the California Current System was investigated. Hindcasts were made from a few hours' to a few days' duration with different extinction profiles from Figure 10b. Differences were calculated in the sea surface temperature, the mixed-layer depth, and the acoustic detection range due to the change in the extinction profile. The mixed-layer depth is defined from the temperature profiles as the depth where the temperature difference between the sea surface and the temperature at depth is equal to 0.2°C . The acoustic detection range is defined as the range at which the transmission loss first exceeds 80 dB. The hindcasts were initialized at 3 hourly intervals over 1 year to provide initialization at different times of the day and at different times of the year. Winds and heat fluxes determined from 3 hourly meteorological observations at Ocean Station November during 1961 were used to provide atmospheric forcing.

Figure 12 shows changes in predicted sea surface temperature, mixed-layer depth, and acoustic detection range for a change in the value of $1/K(490)$ from 30 m to 10 m for mixed-layer hindcasts of 72 hours' duration. Since the hindcasts were conducted every 3 hours, about 240 hindcasts were obtained per month. For the individual hindcasts the magnitude of the differences varied, depending on the particular circumstances of the hindcast.

The predicted sea surface temperature increased as expected—when the turbidity increased. The sea surface temperature showed the highest sensitivity

during the spring and summer heating season when the surface heating is highest, winds are weakest, and the mixed layer is shallowest. The mean bias in the sea surface temperature from May through August is 0.12°C , with the larger peaks being on the order of 0.25°C .

The predicted mixed-layer depth decreased when the turbidity increased. The mixed-layer depth shows the greatest sensitivity to turbidity in winter and spring when it can fluctuate over a relatively large range, e.g., over the upper 100 m or so in this region. The largest differences in mixed-layer depth occur for hindcasts in which the increase in turbidity increases the near-surface thermal stratification sufficiently to form a shallow mixed layer or to keep a shallow mixed layer from deepening.

The changes in acoustic detection range in Figure 12 are calculated using the Passive Raymode acoustic

model for a frequency of 1000 Hz and source and receiver depths of 20 m. Since 1000 Hz requires a sound channel of slightly more than 30 m thickness for ducting, this frequency should be sensitive to near-surface stratification and, hence, turbidity during most of the year. Interestingly, acoustic detection range can increase or decrease with an increase in turbidity. On the average, the acoustic detection range tends to decrease due to a reduction in the thickness of the near-surface sound channel. However, an increase in the near-surface stratification can also improve ducting conditions in a surface or subsurface channel by several means (Urlick, 1975).

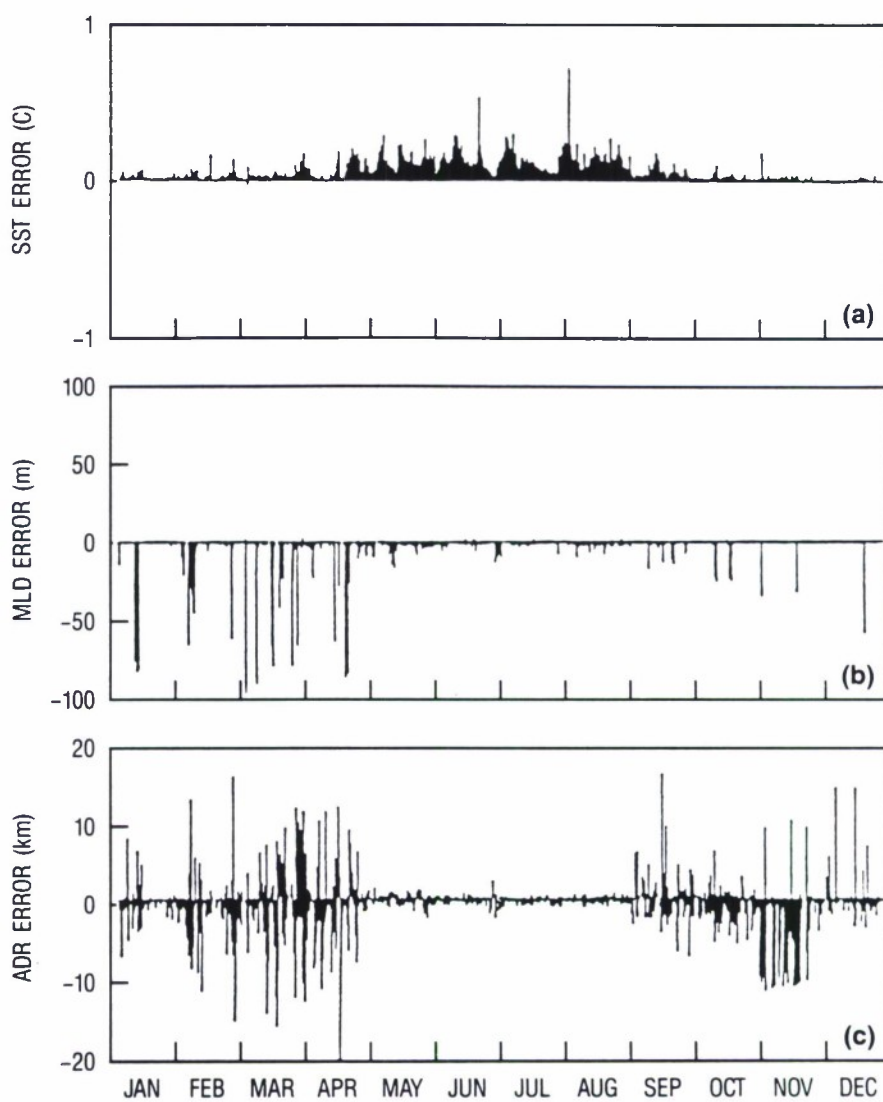


Figure 12. Differences in (a) SST, (b) MLD, and (c) ADR for 36-hour mixed-layer hindcasts due to a change in the extinction profile for solar radiation from that based on a surface value of $1/K(490) = 30\text{ m}$ to that based on a surface value of $1/K(490) = 10\text{ m}$. The ADR was calculated for a frequency of 1000 Hz and source and receiver depths of 20 m.

The sensitivity of acoustic detection range to the increase in turbidity is highest in March and April (Fig. 12). Like the mixed-layer depth, the surface sound channel is affected by the increasing thermal stratification in the spring. The development of this stratification, which is affected by the water clarity, disrupts and shallows the deep surface sound channel that existed during the winter. In the summer, the strong, shallow thermal stratification inhibits the near-surface ducting of medium and low frequencies and, thus, the variability of the acoustic detection range at 1000 Hz caused by the change in $1/K(490)$ (Fig. 12) is significantly reduced. Frequencies higher than 1000 Hz that can be ducted in a thin sound channel might show a greater sensitivity to turbidity during the summer. In the fall, the deepening of the mixed layer deepens the surface sound channel and allows the ducting of increasingly lower frequencies. The acoustic detection range for 1000 Hz shows increased variability due to the change in turbidity in the fall as ducting increases the detection range of this frequency.

Additional work is needed to better understand and quantify the impact of spatial and temporal variability on ocean color-derived turbidity in various ocean regions. Areas of impact range from the daily variability of upper-ocean structure and acoustic prediction to the long-term storage of heat with its ramifications for the global climate.

G. Daniel Hickman

Robert A. Arnone

Temple H. Fay

Coastal Optics

Abstract: The potential importance of satellite ocean color data in shallow waters for the U.S. Navy programs for Special Warfare, Mine Warfare, and Amphibious Warfare is emphasized. In addition, the Navy has a requirement for aircraft laser bathymetry, the utility of which strongly depends upon the optical clarity of the water. The water clarity data useful for planning optical bathymetry measurements can be obtained from satellite ocean color sensors. High spatial resolution optical sensors, such as obtained using Landsat or Spot, are required to yield bathymetric data useful for hydrographic surveys.

Coastal Optical Properties

Dynamic biological and geological processes cause the coastal optical environment to be highly variable. Understanding the spatial and temporal variability of optical properties in coastal regions is required for such naval operations as Special Warfare, Mine Warfare, and Amphibious Warfare. Predictive environmental models of the water clarity in coastal regions are inadequate, since our understanding of the processes and interactions is limited.

Tides, local storms and other meteorological conditions, river runoff, active beach erosion, and high wave action influence the turbidity in the coastal zone. Bottom sediment is brought back into suspension with the fine particles that are responsible for the majority of light scattering that remain in suspension for a long time. Water clarity is also affected by changing the quantity and distribution of nutrients that are mixed throughout the water column, which in turn affect plankton growth. River runoff in the coastal zone, which may be highly seasonal and is correlated with the meteorological conditions, can tremendously influence water turbidity. The affect of these changing environmental conditions on the final optical climate in shallow waters is not well understood.

Remote sensing ocean color imagery provides an important tool for observing the changing optical conditions in the coastal regions. Aircraft and satellite

ocean color measurements provide wide-area coverage on time scales that can be adjusted to a particular application. Remote sensing data can also be obtained in areas that are physically or politically inaccessible by other means. Hydrographic surveying in coastal areas that supports shallow-water warfare areas is normally time consuming when performed by conventional acoustic sensors from ships and small boats. The Navy's present requirement for hydrographic surveys exceeds 200 ship years of survey time. Remote sensing from airborne or spaceborne platforms by optical sensors can provide the Navy effective tools for rapidly acquiring bathymetric data in shallow waters (< 50 m). Research programs have developed airborne lasers and passive multi-spectral scanner systems for conducting hydrographic surveys (Hickman et al., 1986). The performance of these remote sensing systems in obtaining bathymetric data is limited by the optical properties of the water (Lyzenga, 1978; Arnone, 1983a and 1983b). Knowledge of the optical properties is required in planning naval surveys to efficiently use remote sensing systems. To address this problem, the Navy is developing a global atlas, the *Coastal Optics Planner*, which will provide monthly estimates of water clarity (diffuse attenuation coefficient) (Mueller et al., 1990). The atlas is being constructed using ocean color satellite data from the Coastal Zone Color Scanner (CZCS). The data base for the world's coastlines is available at 20-km resolution on monthly averages from November 1978 to June 1986. This data base was constructed from the

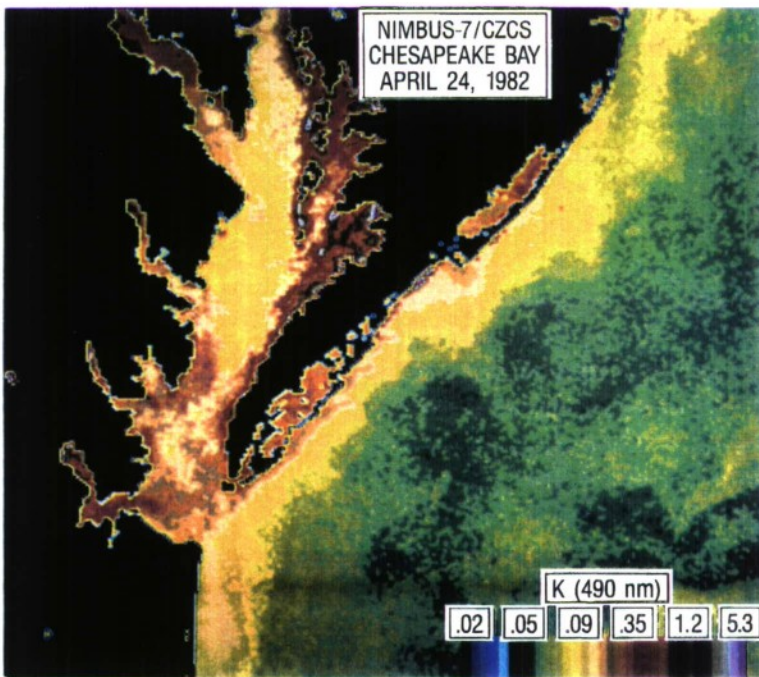


Figure 13. The diffuse attenuation coefficient derived from the CZCS for Chesapeake Bay – 24 April 1982.

Goddard Space Flight Center's global composite imagery (Esaias et al., 1986; Feldman, 1989) and processed on SeaPak (Firestone et al., 1989). Increased resolution to 1-km optical data bases was established for specific regions of naval interest using CZCS ocean color data (Arnone and Oriol, 1985; Oriol and Arnone, 1990). Future planning and operations of naval activities in shallow waters will strongly depend upon optical data, which could be supplied by advanced space-based ocean color sensors (Clark et al., 1986).

Optical properties can be obtained from CZCS data at a 1-km resolution. Figure 13 shows the Chesapeake Bay using an algorithm designed specifically for shallow waters, i.e., capable of discriminating between bottom reflectance and in-water

radiance (Arnone et al., 1990). (Validation of this algorithm is presently being addressed.) This image represents the optical properties for 24 April 1982 at approximately 1100 hours local time. The tides are on ebb when they enter the bay. This figure shows the spatial variability of $K(490)$ values and demonstrates the type of data that would be available for planning naval coastal operations. In this example the dark-red coastal areas ($K(490) > 0.65 \text{ m}^{-1}$) will severely limit use of laser bathymetric systems for hydrographic surveying. Examination of other tidal conditions, seasons, and months indicates the high spatial and temporal variability of the turbidity of the bay. This image shows that the area near the mouth of the bay is more turbid than in the upper bay.

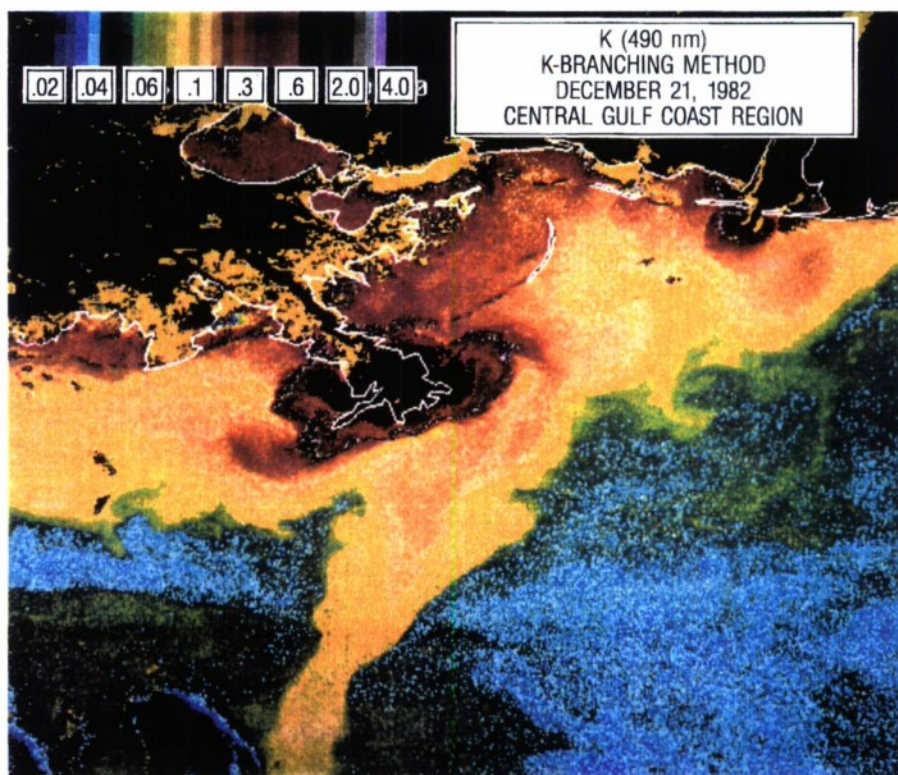


Figure 14. The diffuse attenuation coefficient derived from the CZCS for the Central Gulf Coast Region – 12 December 1982.

Figure 14 illustrates the utility of ocean color for naval coastal operations (Mississippi River plume, December 1982). This figure shows the high variability of the optical environment associated with coastal processes and circulation. The discharge of the Mobile Bay, as shown by the high values of the diffuse attenuation coefficient, appears to move west on its exit from the mouth of the estuary. The complex distribution of the optical properties that surround the Mississippi Delta shows the coastal waters extending well offshore into the Gulf of Mexico. Localized patches of high turbidity appear to be associated with circulation features. Through analysis of sequential imagery of this region, the circulation and evolution of the optical properties can be obtained.

The acquisition of environmental data from inaccessible areas is critical for planning coastal operations. Planning a successful laser bathymetric survey, for instance, would require an understanding of the optical properties of the coastal waters. The influence of the monsoon season on the coastal optical

properties off the Somalia coast is shown in Figures 15a and 15b. (Oriol and Arnone, 1990, compiled a regional optical atlas using 1-km CZCS data). Figure 15a identifies the locations where the optical diffuse attenuation coefficient $K(490)$ was sampled via the CZCS. Figure 15b gives the values of $K(490)$ as a function of monthly averages for selected locations (A, B, C, and D) along the coast. The plot of the monthly $K(490)$ values indicates a significant increase in K during the monsoon season in late fall. The optical data suggest that a laser bathymetric survey should be conducted in spring or summer to optimize results obtained with this technique. In critical operational scenarios, the ability to obtain ocean optical properties in real time from an ocean color satellite would allow optimization of airborne laser bathymetric surveys.

A valuable naval application of aircraft- or satellite-based ocean color, or both, is shallow-water bathymetry. To derive bathymetry from ocean color sensors, much higher spatial resolution scanners, such as exists with Landsat or Spot satellites (30 m and 20 m, respectively) must be used.

Remotely sensed bathymetry from multispectral imagery has been an area of study for some time (Polcyn et al., 1977; Hammack, 1977). Several models were devised to allow the calculation of water depth, including the single-band algorithm (Jerlov, 1976), the dual-band ratio method (Polcyn et al., 1970), the multiband rotational method (Lyzenga, 1978), and the linear multiband technique (Paredes and Spero, 1983). The first two models have the disadvantage of requiring a bottom-type clustering to minimize the sensitivity of the models to bottom reflectance variation. The third model requires knowledge of physical parameters that are generally unknown and the use of bands that may not be available.

The single-band algorithm and the dual-band ratio method have been tested (Clark et al., 1987a; 1987b). Recently, the linear multiband technique of Paredes and Spero has been investigated (Clark et al., 1990). This method has a significant advantage: it does not require preprocessing of the image to cluster and classify bottom types.

Once Landsat computer compatible tapes or other imagery data are read into the computer and converted to an image data file, the data are georeferenced against a large-scale map or chart of the area, i.e., a NOAA or other navigational chart. A set of calibration point soundings digitized from the chart or other data bases, such as National Ocean Survey bathymetry, can be used as ground truth against which to perform the regression.

Once a particular bathymetry model has been calculated, it can be applied over the entire image. This application demonstrates one of the potentially

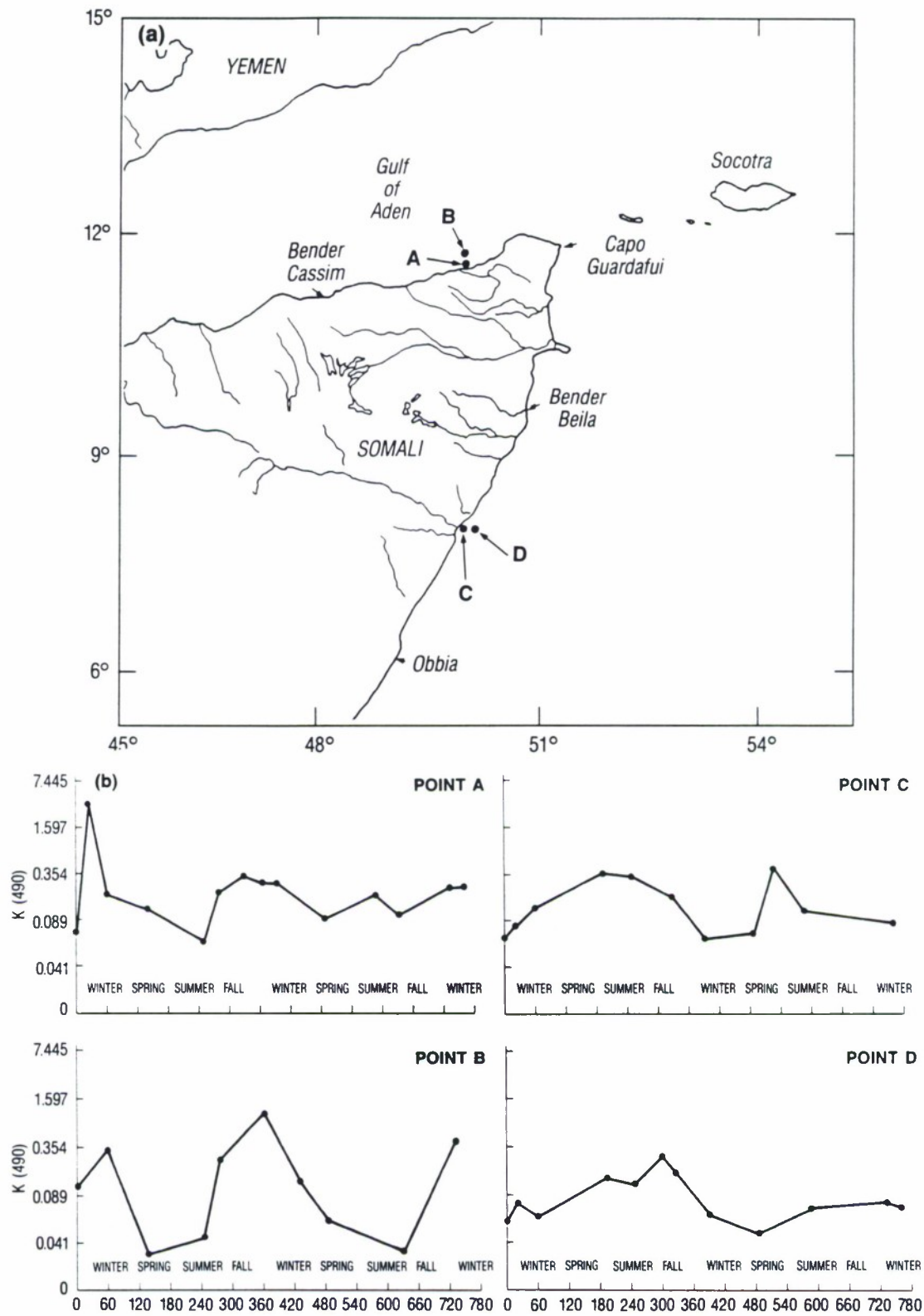


Figure 15. Optical variability off the Somali coast and the Gulf of Aden. (a) Locations where diffuse attenuation coefficient values were derived using CZCS data are marked A→D, and (b) seasonal variations in the diffuse attenuation coefficient at locations A→D.

powerful uses of multispectral bathymetry; i.e., a multispectral bathymetry regression model can be constructed over a relatively small area in which ground truth water depths are available. This model is then applied to a much larger area where perhaps no ground data are available. Research indicates that depths in clear, tropical waters (Bahamas and Vieques) can be calculated to an accuracy of about 1 m to 2 m, or 10% of the depth to a depth of 20 m to 30 m using Landsat thematic mapper imagery.

Figure 16 is a bathymetric chart produced using a thematic mapper image in Vieques. Figure 16a is a composite of the raw blue, green, and red single-band images (channels 1, 2, and 3, respectively) of the thematic mapper image. The coastal bathymetric features can be easily seen due to their lighter colorations. These data were applied to the depth algorithm, and depth estimates were produced (Fig. 16b). Such products as this bathymetric image were used to support a recent naval exercise (Walker et al., 1990).

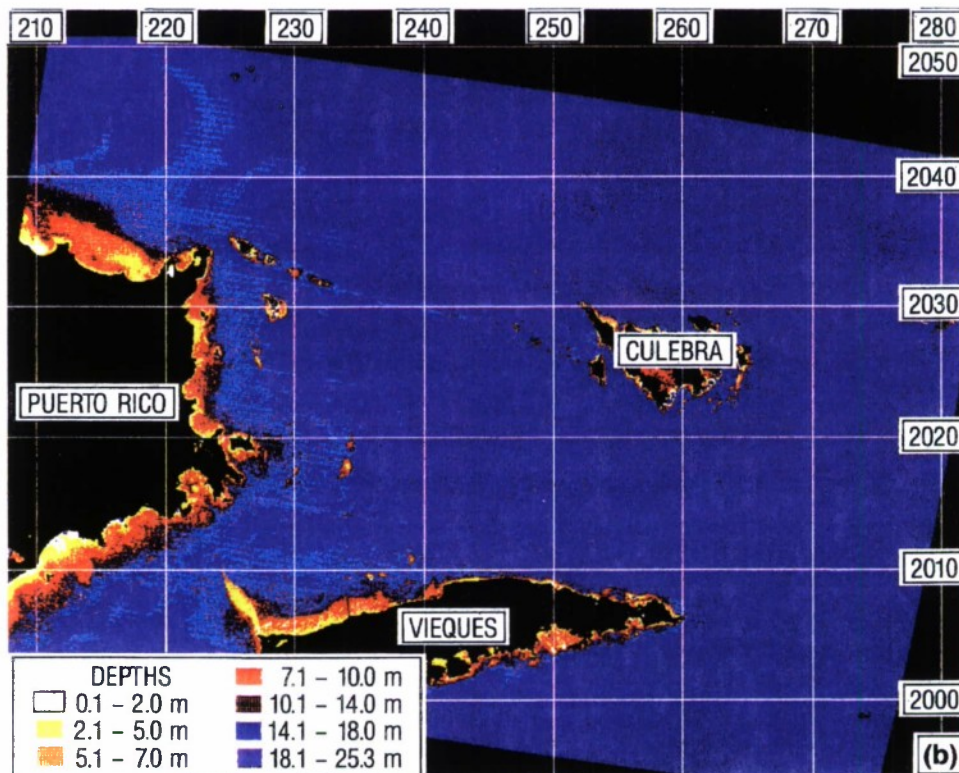
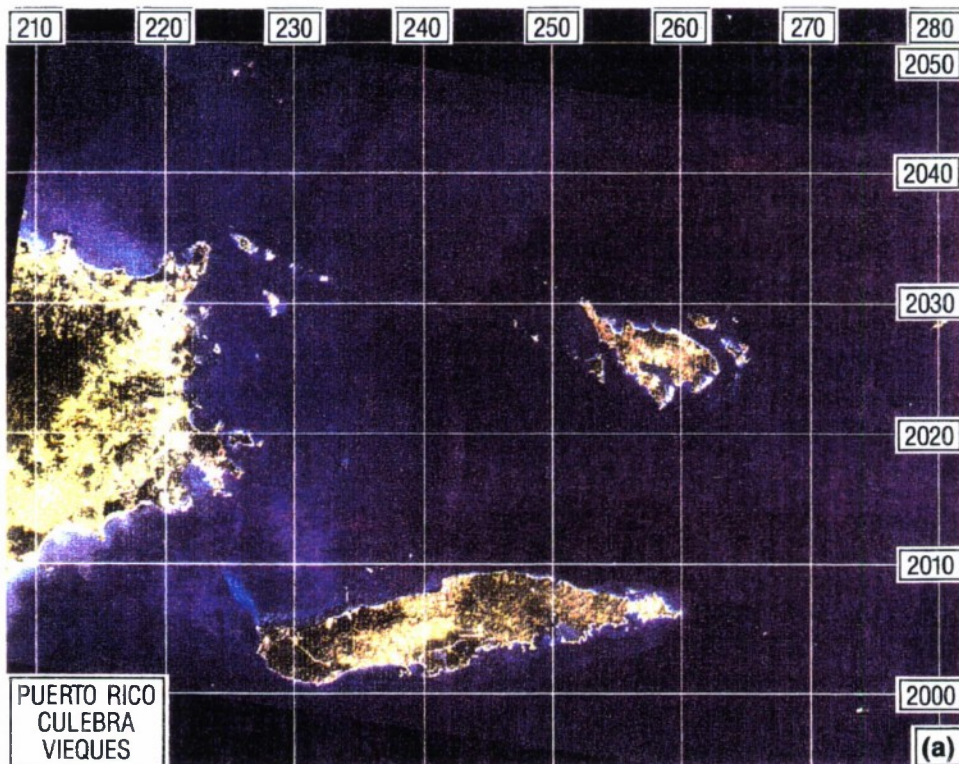


Figure 16. Landsat bathymetry study of Vieques. (a) Composite images of blue, green, and red channels, and (b) bathymetry map calculated using a 3-band regression model.

David K. Young

David Lapota

G. Daniel Hickman

Ocean Color Effects on the Operation of Active and Passive Optical Aircraft/Satellite Systems

Abstract: The knowledge of the optical climatology of the world's oceans is required for active and passive aircraft and satellite systems. This knowledge can be derived only from ocean color satellite systems. Several active laser systems are under development that require this type of data for operational systems. Bioluminescence studies show that satellite ocean color imagery can be an effective predictor of bioluminescence potential if knowledge of forcing functions of the physical environment on primary biological production is sufficient. The relationship between chlorophyll and bioluminescence is deemed to be region specific. Satellite maps of bioluminescence potential (based on ocean color data) would support U.S. Navy requirements.

The performance of aircraft and satellite optical detection (visible) systems requires a detailed knowledge of the optical climate of the world's oceans. Two naval applications have this requirement: active lasers operated from aircraft, satellite, and underwater platforms; and passive detection of bioluminescence. Each area is discussed for deep-water application (see previous article for shallow-water application). Details on specific naval systems will appear in a separate classified document.

Active Lasers

The potential application of operating active lasers aboard aircraft, satellites, and submarines has been investigated for the past 20 years by various countries, including the United States, for a variety of defense and nondefense applications. One such program was the Satellite Laser Communication project. An important product of this program was the design and construction of analytical models to predict the operation and capability of one-way communications between satellites and submarines. The critical environmental

component that affects this laser link is the optical clarity of both the atmosphere and the water.

Limited optical in situ measurements and Coastal Zone Color Scanner (CZCS) data were merged in the derivation and validation of the Satellite Laser Communication Evaluation Algorithm (Naval Ocean Systems Center, 1989a; 1989b). This algorithm is a complex model that deals with issues of atmospheric and oceanic optical propagation over many different scattering regimes. It attempts to model propagation over day and night, over all seasons, for weather, and over all submarine operating areas. The model calculates the predicted signal level at the submarine in joules per centimeters squared. The model's development was a major research effort, and in spite of the acknowledged limitations, it remains fairly robust. Additional ocean color data that could be supplied by future satellite ocean color sensors, such as the Sea-viewing Wide-Field-of-View Sensor (SeaWiFS), will be used to upgrade this important Navy oceanographic / atmospheric model for real-time operation.

Oceanographic data derived from satellite ocean color sensors and the resultant model development is important to both satellite and aircraft communication systems. These systems are potentially important Navy communication networks that have stringent requirements for the type of oceanographic optical data provided by space-based ocean color sensors.

A current program exists within the Air Defense Initiative to investigate the feasibility of developing the performance and prediction capability for optical systems, including but not limited to, lasers. Other active laser programs within the Navy have requirements for the global ocean optical climate, the type of data that can be derived only from satellite-oriented ocean color sensors.

Passive Estimation of Bioluminescence

Bioluminescence potential is defined as the bioluminescence produced by the organisms in a volume of water that is continuously mechanically stimulated until no further light is produced (Rudyakov, 1968). This definition is not always operationally realistic because of limited residence times of stimulated volumes of water in many of the current bathyphotometers (in situ profiling instruments that measure bioluminescence intensity). When dinoflagellates (a common, diverse group of plankton with flash rates measured in milliseconds) predominate among bioluminescent organisms in a water column, correlations between numerical abundances of dinoflagellates and bioluminescence are good. When zooplankton (heterotrophic plankton with intense, long-duration flashes of several seconds or more) predominate, however, correlations may be

poor between abundances of zooplankton and bioluminescence (Batchelder et al., 1990). Studies were conducted in two latitudinally different areas: a November 1981 cruise in the Gulf of California (Lieberman et al., 1987) and an August 1986 cruise in Vestfjord, Norway (Lapota et al., 1989). Strong correlations were found between chlorophyll *a* and bioluminescence.

It has been generalized that increased bioluminescence potential is usually associated with areas of high biological production in the ocean. High biological production is reflected by high chlorophyll values, which can be derived from satellite ocean color imagery. Although intuitively expected, the exact nature of the relationship between chlorophyll and bioluminescence remains unknown (Pressman et al., 1989).

The most recent bioluminescence data were obtained during USNS *Bartlett* Cruise 1312-89 to Vestfjord, Norway, in October 1989. This cruise provided the opportunity to collect continuously pumped seawater from a 3-m depth while the ship was underway. The water columns to 100-m depth at five stations (Fig. 17) within Vestfjord were repeatedly profiled with a bathyphotometer that measured in situ bioluminescence intensities, chlorophyll fluorescence, beam attenuation coefficient, and seawater temperature.

The vertical distribution of water masses within Vestfjord were described by Furnes and Sundby (1981). In the spring, a cold, homogeneous, mixed surface layer is underlain by a 10- to 50-m thermocline where temperature can increase from 4° to 6.5°C. The deeper water is of Atlantic origin and ranges from 6° to 7°C. Seasonal thermoclines during the warmer summer months create a shallow mixed layer where temperatures range from 10° to 15°C. The surface stratified condition persists into October when meteorological lows may cause deepening of the mixed layer by wind-wave activity. Profiles of diffuse attenuation coefficient (*K*) derived from measurements of downwelling irradiance show greatest light attenuation in the upper 30 m of water coincident with the surface mixed layer. One attenuation length ranges from 9.6 to 12.9 m.

In the October 1989 cruise, underway transits were made from Trondheim to Vestfjord, where five stations were investigated:

- in the mouth of the Vestfjord (Station 2);
- along the western margin of the fjord (Station 4);
- in the central fjord (Station 5);
- along the eastern margin of the fjord (Station 1);
- at the head of the fjord (Station 6).

Station 3, previously sampled in 1986 (Lapota et al., 1989), was not sampled during the 1989 cruise but is similar to Station 2 in bio-optical and hydrographic characteristics.

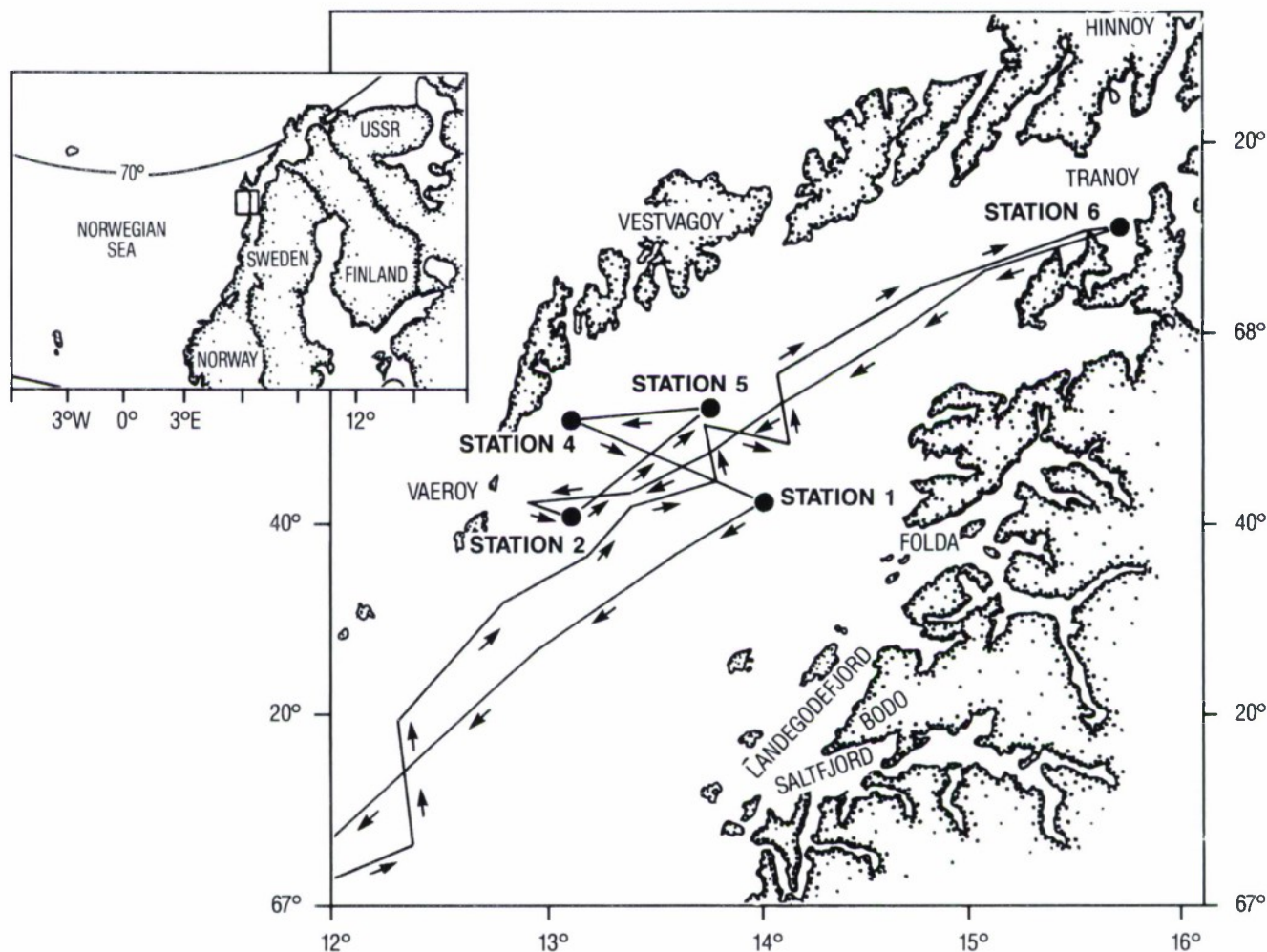


Figure 17. Station locations in Vestfjord, Norway, during BARTLETT 1312-89 Cruise – 5–15 October 1989.

Measured profiles of chlorophyll fluorescence, beam attenuation coefficient, temperature, and bioluminescence show three (Fig. 18) different water types: 1, 2, and 3. Type 1 water was characterized as having the lowest number of bioluminescent dinoflagellates. Type 2 water was characterized as having an intermediate number of bioluminescent dinoflagellates. Type 3 water was characterized as having the highest integrated water-column bioluminescence (equated here with bioluminescence potential) dominated by dinoflagellates with few bioluminescent zooplankton below a 40-m depth.

Type 1 water exhibited the lowest bioluminescent potential but the highest values of chlorophyll fluorescence (Fig. 18a). Both stations 2 and 5, which are representative of this type, were positioned in the open fjord where zooplankton

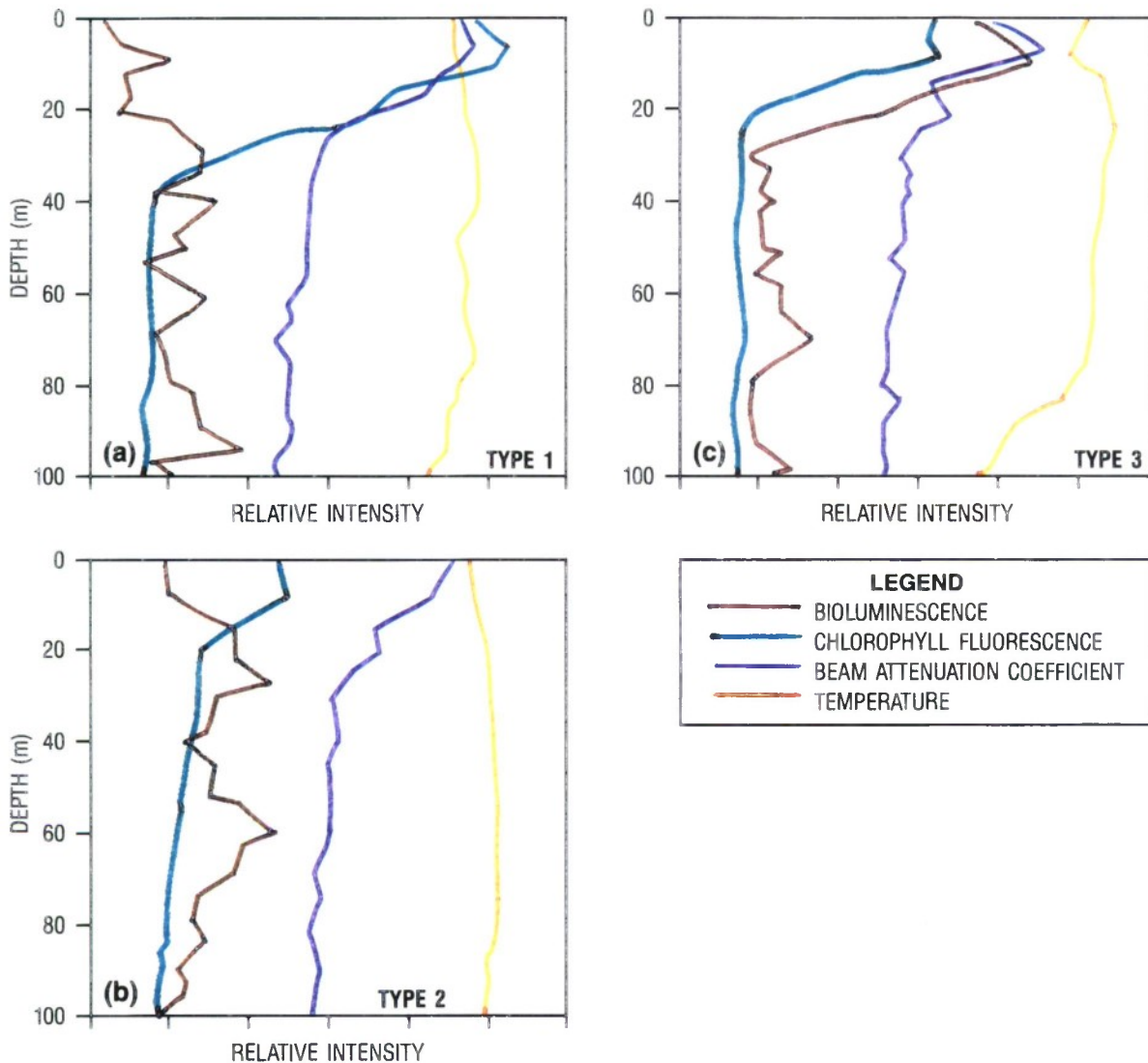


Figure 18. Vertical profiles of bioluminescence intensity and chlorophyll fluorescence measured near midnight in Vestfjord in October 1989. (a) Station 2, (b) Station 1, and (c) Station 6.

contributed up to 50% of the total measured bioluminescence at any given depth to 100 m. Correlations between bioluminescence and numbers of bioluminescent dinoflagellates and chlorophyll fluorescence were poor.

Type 2 water (represented by Station 1) exhibited an intermediate bioluminescence potential and showed no bioluminescence stratification (Fig. 18b). The uniform bioluminescent profile reflects turbulent mixing, which results from winds associated with low-pressure fronts common to the area in the fall. Correlations between bioluminescence and chlorophyll fluorescence

were poor. Zooplankton bioluminescence (largely from copepods, ostracods, and larvaceans) contributed to the bioluminescence profile throughout the water column to a 100-m depth (but never more than 20% of the total bioluminescence at any given depth).

Type 3 water was indicative of the upper fjord conditions, and water of the western fjord demonstrated high amounts of bioluminescence in the upper 10 to 20 m. These findings coincided with a shallow thermocline, and correlations between bioluminescence intensities and chlorophyll fluorescence were strong. This water type is reflective of fjord water in which plankton blooms (dominated by the photosynthetic dinoflagellate *Ceratium fusus*) were responding to thermally stratified outflow from the upper fjord (Fig. 18c; Station 6) and upwelled water of Atlantic origin along the western part of the fjord bounded by the Lofoten Islands (Station 4). During fall, irregularly occurring patches of phytoplankton blooms, which resulted from upwelled water, are predominant in the Norwegian coastal current during the fall (Sakshaug et al., 1981). Such upwelling has been reported for Vestfjord waters during southwest winds (Furnes and Sundby, 1981).

In summary, water types 1, 2, and 3 exhibited the lowest, intermediate, and greatest numbers of bioluminescent dinoflagellates, respectively. Strongest correlations were observed among bioluminescence intensity, chlorophyll fluorescence, and the number of bioluminescent dinoflagellates at type 3 stations. Weaker correlations were observed for type 1 and type 2 stations, where mixed dinoflagellate-zooplankton populations contributed to the bioluminescence profiles. Chlorophyll fluorescence was highly correlated with beam attenuation for all station types. Type 2 stations exhibited a strong correlation between chlorophyll fluorescence and temperature. Beam attenuation, chlorophyll fluorescence, and bioluminescence apparently correlate with one another, as long as the bioluminescence potential is predominantly dinoflagellate in origin. These correlations with bioluminescence degrade as the dinoflagellate contribution to bioluminescence decreases relative to the contribution from zooplankton.

Clearly, the chlorophyll content of seawater estimated from satellite ocean color imagery could be used to predict the bioluminescence potential of the water column for type 3 water in the Vestfjord during fall. As noted, type 3 water was characterized by high biological production of surface stratified water with bioluminescence dominated by contributions from dinoflagellates. Estimates from imagery of type 2 and type 1 water would less accurately predict the bioluminescence potential of these types of water columns in which increasing amounts of bioluminescence were contributed from nonchlorophyll-bearing zooplankton. During summer periods of high biological productivity, decreased

wind-wave activity, and increased water column stratification, satellite imagery could be more effectively used to predict bioluminescence potential from estimated chlorophyll than during the fall. The reasonably high correlations between bioluminescence and chlorophyll measured from underway transects in Vestfjord suggest that estimated chlorophyll from satellite imagery could be an accurate predictor of the bioluminescence potential of surface water.

The data base used in this case study is unusually comprehensive because the spatial and temporal coverage of measured oceanographic variables and bioluminescence intensities are coupled with plankton population characteristics. The data base is also unusual because the seasonal response of oceanic bioluminescence measurements at northern latitudes is relatively unknown. Few bioluminescence measurements have been collected in waters above the Arctic Circle and only during a limited period with respect to the seasonal time scale. Using satellite ocean color in the northern latitudes is always difficult because clouds and fog (particularly along coastal areas) obscure large areas at any given time. However, if “windows of opportunity” present themselves, it is useful to evaluate this data base to explore the potential application of such imagery to gain information on the spatial and temporal variability of bioluminescence potential in these remote waters.

References

Alexander, R. C. and J. W. Kim (1976). Diagnostic model study of mixed layer depths in the summer of North Pacific. *Journal of Physical Oceanography* 6: 293–298.

Arnone, R. A. (1987). Satellite derived color-temperature relationship in the Alboran Sea. *Remote Sensing of Environment* 23: 417–437.

Arnone, R. A. and R. A. Oriol (1985). CZCS Atlas of Water Optical Properties in the Alboran Sea. Naval Ocean Research and Development Laboratory, Stennis Space Center, MS, NORDA Report 117.

Arnone, R. A., R. A. Oriol, C. C. Trees, and J. L. Mueller (1990). Bottom reflectance discrimination using water leaving radiance from Coastal Zone Color Scanner. Proceedings, *International Society for Optical Engineering, Optics X*, Orlando, Florida.

Arnone, R. A. (1983a). Secchi Depth Atlas of World Coastline. Naval Ocean Research and Development Activity, Stennis Space Center, MS, NORDA Report 83.

Arnone, R. A. (1983b). Evaluation of CZCS and Landsat for coastal optics and water properties. *Proceedings, 17th International Symposium of Remote Sensing of Environment*, Ann Arbor, Michigan, May 9–13.

Austin, R. W. and T. J. Petzold (1981). The Determination of the Diffuse Attenuation Coefficient of Seawater Using the Coastal Zone Color Scanner. In *Oceanography from Space*, J. F. R. Gower (ed.), Plenum Publishing Company, Vol. 13, pp. 239–256.

Austin, R. W. and T. J. Petzold (1986). Spectral dependence of the diffuse attenuation coefficient of light in ocean waters. *Optical Engineering* 25: 471–479.

Batchelder, H. P., E. Swift, and J. R. Vankeuren (1990). Pattern of planktonic bioluminescence in the Northern Sargasso Sea; seasonal and vertical distribution. *Marine Biology* 104: 153–164.

Clark, R. K., T. H. Fay, and C. L. Walker (1986). Applications of multispectral imagery to the production of MC&G products. *Proceedings of the Eleventh Annual Department of Defense Mapping, Charting and Geodesy Conference*, Cameron Station, Arlington, Virginia, October.

Clark, R. K., T. H. Fay, and C. L. Walker (1987a). Bathymetry calibration from Landsat TM Imagery under a generalized ratio assumption. *Applied Optics* 26(19): 4036.

Clark, R. K., T. H. Fay, and C. L. Walker (1987b). Bathymetry Measurements from Landsat Imagery in the Vicinity of Isla de Vieques. Naval Ocean Research and Development Activity, Stennis Space Center, MS, NORDA Report 202.

Clark, R. K., T. H. Fay, and C. L. Walker (1990). Shallow Water Bathymetry Models Using Multispectral Digital Imagery. *Journal of Imaging Technology* 16: 170–175.

Cullen, J. J. and R. W. Eppley (1981). Chlorophyll maximum layers of the Southern California bight and possible mechanisms of their formation and maintenance. *Oceanologia Acta* 4(1): 23–32.

Denman, K. L. and M. Miyake (1973). Upper layer modification at Ocean Station Papa: observations and simulation. *Journal of Physical Oceanography* 3: 185–196.

Esaias, W., G. Feldman, C. McClain, and J. Elrod (1986). Monthly satellite-derived phytoplankton pigment distribution for the North Atlantic Ocean Basin. American Geophysical Union, *EOS* 67: 835–837.

Feldman, G. (1989). Ocean color. American Geophysical Union, *EOS* 70(23): 634.

Firestone, J., G. Fu, J. Chen, M. Darzi, and C. McClain (1989). pc-Seapak: a state of the art image display and analyses system for NASA's oceanographic research program. *Proceedings, Fifth Conference on Interactive and Information Processing Systems for Meteorology, Hydrography, and Oceanography*, American Meteorological Society, Anaheim, CA, 29 January–3 February.

Furnes, G. K. and S. Sundby (1981). Upwelling and wind-induced circulation in Vestfjorden. In *The Norwegian Coastal Current*, Norwegian Coastal Current Symposium, Geilo, Norway, Vol. 1. University of Bergen: 152–177.

Gordon, H. R., J. W. Brown, and R. H. Evans (1988). Exact Rayleigh scattering calculations for use with Nimbus-7 coastal zone color scanner. *Applied Optics* 27: 863–871.

-
- Gordon, Howard R., Dennis K. Clark, James L. Mueller, and Warren A. Hovis (1980). Phytoplankton pigments from the Nimbus-7 Coastal Zone Color Scanner: comparisons with surface measurements. *Science* 210: 63–66.
- Gordon, H. R., D. K. Clark, J. W. Brown, O. B. Brown, R. H. Evans, and W. W. Broenkow (1983). Phytoplankton pigment concentrations in the middle Atlantic bight: comparison of ship determinations and CZCS estimates. *Applied Optics* 22(1): 20–36.
- Gordon, H. R. and W. R. McCluney (1975). Estimations of the depth of sunlight penetration in the sea in remote sensing. *Applied Optics* 14(2): 413–446.
- Hammack, J. (1977). Landsat goes to sea. *Photogrammetric Engineering and Remote Sensing* 43: 683.
- Hickman, G. D., M. M. Harris, D. L. Durham, and R. K. Clark (1986). The airborne bathymetric survey system. *MTS Journal* 20(5): 513.
- Jerlov, N. G. (1976). *Optical Oceanography*. New York: Elsevier.
- Kraus, E. B. and J. S. Turner (1967). A one-dimensional model of the seasonal thermocline, 2, the general theory and its consequence. *Tellus* 19: 98–105.
- Lapota, D. M., M. L. Geiger, A. V. Stiffey, D. E. Rosenberger, and D. K. Young (1989). Correlations of planktonic bioluminescence with other oceanographic parameters from a Norwegian fjord. *Marine Ecology Progress Series* 55: 217–227.
- Lieberman, S. H., D. Lapota, J. R. Losee, and A. Zirino (1987). Planktonic bioluminescence in the surface waters of the Gulf of California. *Biol. Oceanogr.* 4: 25–46.
- Lyzenga, D. R. (1978). Passive remote sensing techniques for mapping water depth and bottom features. *Applied Optics* 17: 379.
- Martin, P. J. (1985). Simulation of the mixed layer at OWS N and P with several models. *Journal of Geophysical Research* 90: 903–916.
- Morel, A. and L. Prieur (1977). Analysis of variations in ocean color. *Limnology and Oceanography* 22(4): 709–722.
- Mueller, J. L., C. C. Trees, and R. A. Arnone (1990). Evaluation of Coastal Zone Color Scanner diffuse attenuation coefficient algorithms for application to coastal waters. *Proceedings, Ocean Optics X*, 16–18 April.
-

Mueller, J. L. and R. L. Lange (1989). Bio-optical provinces of the northeast Pacific Ocean: a provisional analysis. *Limnology and Oceanography* 34(8): 1572–1586.

Naval Ocean Systems Center (1989a). Satellite Laser Communications Evaluation (SLCEVAL): Model Description and Validation. Naval Ocean System Center (Code 844), San Diego, CA.

Naval Ocean Systems Center (1989b). Satellite Laser Communications Evaluation Algorithm (SLCEVAL): independent validation and verifications (IV and V). Naval Ocean Systems Center, San Diego, CA, final report, November.

Oriol, R. A. and Arnone, R. A. (1990). Seasonal Optical Properties Derived from Coastal Zone Color Scanner Data Along the Somali Coast and the Gulf of Aden. Naval Ocean Research and Development Activity, Stennis Space Center, MS, NORDA Report 244.

Paredes, J. M. and R. E. Spero (1983). Water depth mapping from passive remote sensing data under a generalized ratio assumption. *Applied Optics* 22, (8): 1134.

Polcyn, F. C., W. L. Brown and I. J. Sattinger (1970). The Measurement of Water Depth by Remote Sensing Techniques. Willow Run Laboratories, The University of Michigan, Ann Arbor, MI, Report 8974–26–F.

Polcyn, F. C., D. R. Lyzenga, and F. J. Tanis (1977). Demonstration of Satellite Bathymetric Mapping. Environmental Research Institute of Michigan, Ann Arbor, MI, Report 122200–1–F.

Pressman, A. E., R. J. Holyer, J. L. Mueller, J. M. Harding, P. J. Martin, R. A. Arnone, and J. E. Curtis (1989). Application of Satellite Ocean Color Imagery: Plan and Workshop Report. Naval Ocean Research and Development Activity, Stennis Space Center, MS, NORDA SP 080:321:89.

Rudyakov, Y. A. (1968). Bioluminescence potential and its relation to concentration of luminescent plankton. *Oceanology* 8: 710–715.

Rutkovskaya, V. A. and E. N. Khalemskiy (1973). Calculating the depth of penetration of solar energy in seawater (with the Pacific as an example), *Oceanology* 14: 398–404.

Sakshaug, E., S. Myklestad, K. Andresen, E. M. Hegseth, N., and L. Jorgensen (1981). Phytoplankton off the More coast in 1975–1979: distribution, species composition, chemical composition and conditions for growth. In *The Norwegian Coastal Current*, Norwegian Coastal Current Symposium, Geilo, Norway, University of Bergen, vol. II, pp. 681–711.

Schmidt, R. W. and D. B. Olson (1985). Wintertime convection in warm-core rings: thermocline ventilation and the formation of mesoscale lenses. *Journal of Geophysical Research* 90(C5): 8823–8838.

Simpson, J. J. and T. T. Dickey (1981). The relationship between downward irradiance and upper ocean structure. *Journal of Physical Oceanography* 11: 309–323.

Smith, R. C. and K. S. Baker (1982). Oceanic chlorophyll concentrations as determined by satellite (Nimbus 7 CZCS). *Marine Biology* 66: 269–279.

Smith, R. S. and K. S. Baker (1978). The bio-optical state of ocean waters and remote sensing. *Limnology and Oceanography* 23(2).

Urick, R. J. (1975). *Principles of Underwater Sound*. New York (NY): McGraw-Hill Book Company.

Walker, C. L., D. Byman, M. T. Kalcic, and T. Beaubouef (1990). Multispectral Imagery Support for Ocean Venture 90. Naval Oceanographic and Atmospheric Research Laboratory, Stennis Space Center, MS, SP 058:351:90.

REPORT DOCUMENTATION PAGE

Form Approved
OMB No. 0704-0188

Public reporting burden for this collection of information is estimated to average 1 hour per response, including the time for reviewing instructions, searching existing data sources, gathering and maintaining the data needed, and completing and reviewing the collection of information. Send comments regarding this burden estimate or any other aspect of this collection of information, including suggestions for reducing this burden, to Washington Headquarters Services, Directorate for Information Operations and Reports, 1215 Jefferson Davis Highway, Suite 1204, Arlington, VA 22202-4302, and to the Office of Management and Budget, Paperwork Reduction Project (0704-0188), Washington, DC 20503.

1. Agency Use Only (Leave blank).		2. Report Date. May 1992		3. Report Type and Dates Covered. Final	
4. Title and Subtitle. Applications of Ocean Color to Naval Warfare			5. Funding Numbers. Job Order No. 93211L Program Element No. 0603704N Project No. 0101 Task No. 100 Accession No. DN258120		
6. Author(s). G. D. Hickman, R. A. Arnone, T. H. Fay, J. M. Harding, P. J. Martin, D. K. Young D. Lapota*, J. L. Mueller**					
7. Performing Organization Name(s) and Address(es). Naval Oceanographic and Atmospheric Research Laboratory Ocean Science Directorate Stennis Space Center, Mississippi 39529-5004			8. Performing Organization Report Number. BC 009:91:321		
9. Sponsoring/Monitoring Agency Name(s) and Address(es). Space and Naval Warfare Systems Command Washington, DC.			10. Sponsoring/Monitoring Agency Report Number.		
11. Supplementary Notes. *Naval Ocean Systems Center, San Diego, California **State University of San Diego, San Diego, California					
12a. Distribution/Availability Statement. Approved for public release; distribution is unlimited. Naval Oceanographic and Atmospheric Research Laboratory, Stennis Space Center, MS 39529-5004.			12b. Distribution Code.		
13. Abstract (Maximum 200 words). <small>Remotely sensed ocean color technology offers the Navy a new source of environmental information to support U.S. Navy warfare operations and planning. Potential naval applications of ocean color were reviewed in a recent workshop report (Pressman et al., 1989). This publication gives examples of ocean color applications that satisfy well-recognized requirements for oceanographic information in naval warfare activities. The technology behind these examples is sufficiently mature to allow near-term development of naval applications to use the new satellite ocean color instrument, the Sea-viewing Wide-Field-of-View Sensor (SeaWiFS), beginning in 1993. Operational implementations of these "naval applications" will be based on real-time satellite ocean color imagery, backed up by optical climatologies derived through offline analyses. Ocean color is the spectral reflectance of the water column. It is measured remotely as wavelength-dependent radiance emerging from the sea surface. Ratios of water-leaving radiances are used to calculate phytoplankton pigment concentration (Gordon et al., 1983), and optical diffuse attenuation coefficients (Austin and Petzold, 1981; Mueller et al., 1990). When ocean color is measured from space using images composed of visible wavelengths, up to 85% of the radiance measured in the 0.45 to 0.55 μm region is sunlight that is scattered backward by the earth's atmosphere. The atmosphere also attenuates the water-leaving radiance transmitted from the ocean surface on its path to the sensor. Therefore, atmospheric corrections must be applied to derive accurate ocean color parameters from satellite radiance measurements (Gordon et al., 1983; Gordon et al., 1988). Robust methods for removing atmospheric effects and determining ocean bio-optical properties from ocean color imagery have evolved through a decade of research using the Coastal Zone Color Scanner (CZCS) on board the Nimbus-7 earth-orbiting satellite. The CZCS was a multispectral, imaging radiometer placed in operation on Nimbus-7 in October 1978. This instrument was designed to measure subtle variations in ocean color in four narrow wavelength bands. Its special features included finer spectral resolution, better radiometric sensitivity, and higher signal-to-noise ratios than previous satellite radiometers. The CZCS scan view could also be tilted backward or forward along the subsatellite track to avoid sunglint contamination. The CZCS was turned on several times daily for brief periods (up to 120 minutes a day) and continued successful operation through mid-1986, a span far longer than its 1-year design life. Researchers are currently attempting to exploit this rich data set for numerous applications, including those of major interest to the U.S. Navy. Research using CZCS data established the feasibility of using ocean color observations from space to study global and mesoscale distributions of ocean bio-optical properties. NASA recently signed a contract to develop and fly a second generation satellite ocean color imaging system (SeaWiFS). The SeaWiFS ocean color instrument is designed with eight channels in the visible and near-infrared regions of the electromagnetic spectrum. Four of the visible SeaWiFS channels are similar to those of the CZCS. SeaWiFS will operate globally on a 100% daylight duty cycle, which makes it suitable for the Navy and other real-time operational users, as well as for post processing analyses. Subject to user fees, the Navy's existing Advanced Very High Resolution Radiometer High Resolution Picture Transmission (HRPT) communications units (SMO-11 or its successor) will be capable of receiving the SeaWiFS data with only minor modifications. Furthermore, the Navy's Tactical Environmental Satellite System 3 (TESS-3) computer systems will readily handle naval applications analyses of satellite ocean color image data. SeaWiFS will give the Navy a highly cost-effective way to obtain valuable environmental information (compared to developing a dedicated sensor system). The section on "Optical Climatologies" gives examples of satellite-derived ocean color images that have been shown to yield global information on the visibility of the ocean. This information is valuable for predicting the performance of various naval electro-optical applications, such as aircraft or satellite-to-submarine communications, and performance predictions applicable to a variety of detectors and/or imaging electro-optical systems in nonacoustic antisubmarine warfare, mine warfare, and bathymetric mapping (see sections on "Coastal Optics" and "Ocean Color Effects on the Operation of Active and Passive Optical Aircraft/Satellite Systems"). "Ocean Color Visualization of Mesoscale Water-Mass Features" previews examples of ocean color. These examples clearly identify mesoscale ocean fronts and eddy features (critical to acoustic predictions for antisubmarine warfare) that are similar to those derived from sea surface temperature. In some cases, however, mesoscale features exist but lack sea surface thermal signatures. These features, when resulting from changes in chlorophyll concentration or turbidity variations, can be observed with ocean color sensors. Ocean color can be valuable in those locations where the atmosphere is so humid that the infrared derived sea surface temperature measurements are useless due to strong absorptions of the infrared by the water vapor. Mesoscale features have been observed via ocean color in areas where the changes in the chlorophyll levels are mainly caused by salinity and not temperature gradients. Such features would go undetected using only sea surface temperatures. "Sensitivity of the Prediction of Upper-Ocean Thermal Structure to Turbidity Estimated from Ocean Color" illustrates that variations in seawater turbidity detected via ocean color can affect the ocean thermal structure on seasonal time scales. Thermal structure changes can result in significant variability in the acoustics at strong water mass boundaries, which in turn can affect sea surface temperature, mixed layer depth, and acoustic detection range. Although the majority of the research effort on the use of ocean color for naval applications has been involved with deep-water oceanography using CZCS data, examples derived from both aircraft and satellite sensors show (see "Coastal Optics") ocean color extended into shallow water. Once appropriate algorithms are developed for (including validations) shallow water, many naval applications (e.g., Mine Warfare, Amphibious Warfare, and Hydrographic Bathymetric Surveying) can greatly profit from the optical sensors. The examples given in this report show that aircraft and satellite ocean color derived products can be used in conjunction with other remote sensor and <i>in situ</i> data to solve major naval requirements. Ocean color has matured to the state where many ocean color products are in various stages of development and transitioning to the U.S. Fleet. However, substantial resources—from basic research through advanced development—should be directed towards ocean color. This support is necessary if the Navy is to fully utilize the potential of this new technology for Naval applications.</small>					
14. Subject Terms. ocean color, CZCS, Sea WiFS			15. Number of Pages. 53		
			16. Price Code.		
17. Security Classification of Report. Unclassified		18. Security Classification of This Page. Unclassified		19. Security Classification of Abstract. Unclassified	
			20. Limitation of Abstract. None		